INTERNATIONAL ATOMIC ENERGY AGENCY
UNITED NATIONS EDUCATIONAL, SCIENTIFIC AND CULTURAL ORGANIZATION
INTERNATIONAL CENTRE FOR THEORETICAL PHYSICS
I.C.T.P., P.O. BOX 586, 34100 TRIESTE, ITALY. CABLE CENTRATOM TRIESTE

H4.SMR/854-28

College on Computational Physics

15 May - 9 June 1995

Atomic and Electronic Structure of Clusters from Car-Parrinello Method

V. Kumar

Indira Gandhi Centre for Atomic Research
Kalpakkam, India

MAIN BUILDING STRADA COSTIERA, 11 TEL. 2240111 TELEFAX 224163 TELEX 460392 ADRIATICO GUEST HOUSE VIA GRIGNANO, 9 TEL. 224241 TELEFAX 224531 TELEX 460449
MICROPROCESSOR LAB. VIA BEIRUT, 31 TEL. 224471 TELEFAX 224600 TELEX 460392 GALILEO GUEST HOUSE VIA BEIRUT, 7 TEL. 22401 TELEFAX 2240310 TELEX 460392

IC/94/127

International Atomic Energy Agency
and
United Nations Educational Scientific and Cultural Organization
INTERNATIONAL CENTRE FOR THEORETICAL PHYSICS

ATOMIC AND ELECTRONIC STRUCTURE OF CLUSTERS FROM CAR–PARRINELLO METHOD [1]

Vijay Kumar [2]
International Centre for Theoretical Physics, Trieste, Italy.

MIRAMARE - TRIESTE
June 1994

[1] Chapter in 'Lectures on Methods of Electronic Structure Calculations' eds. V. Kumar, O.K. Anderson and A. Mookerjee, World Scientific, 1994.

[2] Permanent address: Materials Science Division, Indira Gandhi Centre for Atomic Research, Kalpakkam - 603 102, India.

ABSTRACT

With the development of *ab-initio* molecular dynamics method, it has now become possible to study the static and dynamical properties of clusters containing upto a few tens of atoms. Here I present a review of the method within the framework of the density functional theory and pseudopotential approach to represent the electron–ion interaction and discuss some of its applications to clusters. Particular attention is focussed on the structure and bonding properties of clusters as a function of their size. Applications to clusters of alkali metals and Al, non–metal - metal transition in divalent metal clusters, molecular clusters of carbon and Sb are discussed in detail. Some results are also presented on mixed clusters.

1. Introduction

During the past decade much experimental and theoretical progress has been made in our understanding of the physical and chemical properties of several elemental, binary and compound clusters[1–5]. Interest in these studies has basically arisen from the technological importance of clusters e.g. in catalysis, photographic films, magnetic recording, etc. and from the quest to understand the evolution of materials properties as a function of the size of an aggregate. Very recently it has also become possible[6] to prepare a new form of solid carbon from large carbon clusters which are now referred to as fullerenes. These fullerenes are caged structures having 12 pentagons and a varying number of hexagons of carbon atoms. The most beautiful and interesting among these fullerenes is the C_{60} molecule which has the truncated icosahedral structure. These molecules can be crystallized in a $Pa\bar{3}$ structure at low temperatures. The exciting discovery of superconductivity at relatively high temperatures in K^7(18 K), Rb^8(28 K) and Cs and Rb^9(33 K) doped solid C_{60} has provided another dimension to cluster research and efforts are now also being made[10–12] to find other clusters/molecules which could be used as building blocks for making new materials. It has also been possible to encapsulate atoms and molecules within fullerenes[13] and to prepare other forms of carbon such a buckytubes[14] and

bucky onions[15] etc . These developments have therefore broaden the scope of the studies of finite aggregates and opened up new avenues in materials research. Also it is hoped that the progress in cluster research will enhance our understanding of complex structures and pave the way for new molecular architecture.

One of the important factors which governs the properties of clusters is their structure which is in general very different from a bulk fragment. This is due to the fact that in a small cluster most of the atoms are on the surface and therefore have reduced coordination. This leads to a reconstruction of the bulk fragment so that the *free energy* of the cluster becomes minimum. In addition there are quantum effects which lead to an oscillatory behaviour of e.g. the binding energy, ionization potential etc. as the cluster size grows. Such changes in the atomic and electronic structure can affect significantly the bonding and other physical and chemical properties of clusters. Some interesting examples are small clusters of divalent and tetravalent elements. Si clusters have been found to have closed packed structures[16] as compared to strongly directional bonding in the bulk whereas small carbon clusters have structures ranging from chains, rings, fullerenes, tubes, onions and possibly some other forms also. Dimers of divalent metals such as mercury and magnesium are very weakly bonded due to ns^2 closed shell atomic electronic structure and a large promotional energy to the p state but these are good metals in bulk. Therefore for such elements a transition to bulk chemical bonding should occur as the cluster size grows. However, in most cases it is still not clear when such a transition would occur. This may range from a few tens to a few hundred or thousand atoms depending upon the species involved. For mercury, experiments[17] indicate this transition to occur for a moderate size of the clusters ($70 \geq N \geq 13$).

Clusters also differ in an important way from bulk materials when alloyed. In the bulk, alloying is not possible if the atomic size difference is larger than about 15%. However, for clusters there is no such restriction on the relative size of atoms. Thus binary clusters such as Cu-Os could be formed[18]. This provides another interesting way of improving the reactivity and selectivity of clusters by effectively changing the *local* electronic structure. Several studies on the reactivity of clusters illustrate the importance of the variation of the electronic structure with cluster size. Iron clusters have been found to show[19] several orders of magnitude change in the reaction rate of deuterium as the cluster size changes from a few to few tens of atoms. This correlates well with the variation in the electron binding energy of the clusters as shown in Fig. 1. The reactivity increases as the electron binding energy decreases. The latter generally decreases with an oscillatory behaviour to the value of the work function as the cluster size grows. Similarly Al clusters show marked variation in the reactivity with oxygen as a function of their size[20]. The magic clusters Al_{13}^- and Al_{23}^- are found to be unreactive with oxygen whereas the non-magic clusters do react.

The magnetic properties of small clusters are also in general very different from the bulk due to the discrete nature of the electronic energy spectrum. Clusters of elements which are non-magnetic in bulk can possess magnetic moments while in the case of the magnetic elements, the moments can be significantly different from

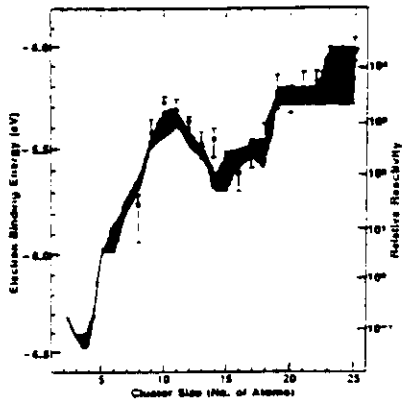

Figure 1: Comparison of electron binding energy and reactivity of Fe_N clusters for dissociative chemisorption of D_2 and H_2. The shaded portion reflects the uncertainty in ionization threshold measurements while the vertical bars indicate uncertainty in reactivity results. (After Whetten et al[19])

their bulk value. Also the different sites in a cluster will in general have different magnetic moments. There is little progress in this direction so far. Similarly due to changes in the charge density distribution, the optical properties of clusters are expected to be different from the behaviour on semi-infinite surfaces. In principle clusters form a much broader class of materials because different clusters of even the *same* material may behave quite differently and in the case of more than one component, the atomic size of the constituents is not the limiting factor. Such studies can therefore help to prepare better catalysts, photographic films, magnetic tapes, energy storage devices, etc. by suitable choices of material and particle size and can open doors for making new classes of materials such as fullerites, the crystals obtained from fullerenes.

Experimentally while direct information on the structure of clusters is difficult, it has been possible to study the ionization energy, magnetic and electric moments, density of states, polarizability, photoabsorption cross section and effects of multiple charging etc. of mass selected clusters. Experiments on mass selected clusters containing upto several thousand atoms have become possible[21]. However, most theoretical studies based on ab-initio methods have been possible on clusters containing a few atoms only since it is difficult to know the lowest energy structures due to the very many atomic and electronic configurations that are possible for a given size of the cluster. Calculations based on a jellium model[22] are simpler and can be done for large clusters. These have been very successful in providing a qualitative understanding of the variations in the stability, ionization potentials, polarizability etc. of clusters of simple metals as a function of their size[4,5]. However, in several

cases of interest such as clusters of semiconductors, transition metals and alloys, a jellium model may not be suitable. Also for a quantitative understanding it is necessary to know the atomic structure and the changes in the electronic structure as a function of the size and geometries and their temperature dependence. This is also likely to enhance our understanding of the dynamical properties, structural transformation and melting etc. of clusters and will be helpful in understanding chemical reactions on clusters.

Theoretical studies (see e.g. Refs. 1-5) of the atomic and electronic structure of clusters of various elements have been numerous. These include studies based on the use of some interatomic potentials as well as ab-initio calculations. While studies based on some interatomic potentials can be done for clusters having upto several thousand atoms and have given some useful information, one has to be cautious about the validity of such results (in particular for small clusters) as potentials generated from some known structures of a material may not be appropriate for other structures of the same material. One can hope to get a good description of clusters of rare gases using pair- potentials whereas interactomic potentials based upon effective medium theories or tight binding methods may particularly be useful for large clusters of metals and semiconductors. Ab-initio calculations are much more difficult and have been possible for clusters having at best upto a few tens of atoms. A majority of these calculations have been done for a fixed atomic distribution in the cluster. However, in several cases the atomic structure has been relaxed and efforts have been made to find structures with lowest energies. These include calculations based on configuration interaction as well as density functional methods. However, most of these have been restricted to clusters with a few atoms only. The most promising development which has given theoretical study of clusters a new perspective, has been the ab-initio molecular dynamics (MD) approach developed by Car and Parrinello[23] (CP). In this appraoch the many body interatomic potential is calculated from ab-initio calculations based upon the density functional theory (see articles by von Barth and M P Das in this volume) which has proved very successful in the study of the structural and electronic properties of a variety of materials. The ab-initio molecular dynamics method not only allows a search of the lowest energy structures within the framework of the simulated annealing (SA) but also it can be used to study the static and dynamical properties of clusters having upto a few tens of atoms. So far its applications have been to clusters of $s-p$ bonded elements. However, recent developments of dealing with the d-orbitals within this scheme (see article by Laasonen in this volume) will make the study of technologically more important clusters with transition metal elements feasible. Some of the systems that have already been studied successfully include clusters[24,26] of Si[17], Se[25], S[27], Na[28,29], P[30], Be[31], Mg[32], Sb[33,34], Sn[35], Al[36,37], Ga[37,38], C[39-41], B[42], Ge[24] and mixed clusters of GaAs, GaP and AlAs[43], NaK[28], Na-Mg[44], Al-Si, Al-C and B-C[45]. Good agreement has been obtained with experimental data wherever available. Here I will discuss the CP method and present results of some of these applications. There are a few other reviews[46-49] on this method which have appeared recently and contain some details of this method and applications to other systems such as liquid and amorphous materials, surface structure, diffusion, defects etc. Some details can also be found in the articles by Pastore and Laasonen in this volume.

In the following section I present the calculational procedure. Section 3 contains a review of most of the results on clusters obtained so far using the ab-initio molecular dynamics procedure. Section 4 contains an outlook for future work.

2. ab-initio Molecular dynamics method

In classical molecular dynamics approach an empirical interatomic potential, often a pairwise interaction, is used to calculate the energy of a system. Such empirical potentials are constructed from a fit to some known properties of that material. However, except for rare gas solids and strongly ionic materials, in most other systems it is difficult to justify a pairwise interaction from first principles. Further, during MD simulation the ionic positions can change very significantly from their starting configuration and structural transformation may occur for which the starting potential may not be valid. In cases such as clusters where the structure of the system is *a priori* not known, it would be difficult even to find a good interatomic potential. Car and Parrinello[23] combined one of the most successful theories of total energy calculation of an aggregate, namely the density functional method[50,51], with the molecular dynamics approach to develop an efficient combined electron-ion minimization procedure. Hereafter we shall refer the methods based on the idea of the density functional molecular dynamics approach to as the ab-initio molecular dynamics methods. In the following we first discuss briefly the Kohn-Sham equations[52] which are central to the solution of the electronic structure problem within the density functional formalism and then describe the standard and the MD approaches for solving these equations.

2.1 Kohn-Sham equations

The density functional theory as developed by Hohenberg and Kohn[50] and Kohn and Sham[51] offers a formal exact treatment of solving the ground state electronic properties of a system. However, it requires the knowledge of a functional for exchange and correlation which is not known for most systems. An approximate treatment of the exchange and correlation energy based on the local density or local spin density approximation (LDA or LSD) has been successfully used in a wide variety of systems ranging from atoms and molecules to surfaces and bulk materials and will also be the basis of the ab-initio MD to be discussed here.

For systems such as clusters one of the principal tasks of an ab-initio calculation is to obtain the lowest energy isomers by minimizing the total energy E with respect to the ionic and electronic degrees of freedom. Within the density functional theory this can be achieved by solving the Kohn-Sham equations (for details see the article by M. P. DAs),

$$[-\frac{1}{2}\nabla^2 + V_{ext}(\mathbf{r}) + V_H(\mathbf{r}) + V_{xc}(\mathbf{r})]\psi_i(\mathbf{r}) = \epsilon_i\psi_i(\mathbf{r}), \quad (1)$$

where V_{ext}, V_H and V_{xc} are the external (electron - ion), Hartree and exchange-correlation potentials respectively (atomic units $e = \hbar = m_e = 1$ are used.). The electron-ion potential can be an all electron or a pseudopotential. The other two contributions to the potential are

$$V_H(\mathbf{r}) = \int d\mathbf{r}' n_e(\mathbf{r}')/|\mathbf{r} - \mathbf{r}'| \quad (2)$$

and

$$V_{xc}(\mathbf{r}) = \frac{dE_{xc}}{dn_e(\mathbf{r})}, \quad (3)$$

where the electronic charge density $n_e(\mathbf{r})$ is given by,

$$n_e(\mathbf{r}) = \sum_i^{occ} f(i)|\psi_i(\mathbf{r})|^2, \quad (4)$$

$f(i)$, being the occupation number for the state i. The ground state total energy E for a given configuration of the ions $\{\mathbf{R}_I\}$ is

$$E[\{\psi_i\},\{\mathbf{R}_I\}] = \sum_i^{occ} f(i)\int d\mathbf{r}\psi_i^*(\mathbf{r})(-\frac{1}{2}\nabla^2)\psi_i(\mathbf{r}) + \int d\mathbf{r}V_{ext}(\mathbf{r})n_e(\mathbf{r})$$

$$+\frac{1}{2}\int d\mathbf{r}d\mathbf{r}'\frac{n_e(\mathbf{r})n_e(\mathbf{r}')}{|\mathbf{r}-\mathbf{r}'|} + E_{xc}[n_e] + \frac{1}{2}\sum_{I\neq J}\frac{Z_I Z_J}{|\mathbf{R}_I - \mathbf{R}_J|}. \quad (5)$$

Here Z_I is the charge on the I^{th} ion at the position $\mathbf{R}_I$. $E_{xc}[n_e]$ is the exchange-correlation energy. This has been calculated within the LDA/LSD in almost all the applications of the ab-initio MD,

$$E_{xc}[n_e] = \int d\mathbf{r}n_e(\mathbf{r})\epsilon_{xc}[n_e(\mathbf{r})], \quad (6)$$

where $\epsilon_{xc}[n_e(\mathbf{r})]$ is the exchange-correlation energy per particle for a homogeneous electron gas with density $n_e(\mathbf{r})$. In the case of spin polarized calculation, this energy should correspond to the density with the same spin polarization as in the actual system. There are several approximate forms available for this and therefore E_{xc} can be easily calculated in real space once the density is known. This approximation yields reliable binding energy trends and equilibrium structures for a variety of molecules[52] and solids[53]. However, recently there have been interesting developments where non-local exchange-correlation functionals have been successfully used which have provided improved agreement with experiments for several systems (see von Barth in this volume). Their inclusion in the ab-initio MD scheme

is also likely to give improved results but since most applications have been done within LDA/LSD we shall restrict our discussion to LDA/LSD only.

2.1.1 The standard approach

In the standard approach, for a given configuration of the ions, one has to guess a starting wavefunction, construct the Hamiltonian matrix and then solve (1) iteratively untill self-consistency is achieved. One can then use the steepest descent technique to relax the ionic positions by calculating the forces on ions,

$$\mathbf{F}_I = -\frac{\delta E}{\delta \mathbf{R}_I} \quad (7)$$

following the Hellman-Feynman theorem[54]. This would lead to a *local* minimum in the energy surface. However, for finding global minimum one has to then take a new configuration and repeat this procedure until a configuration is obtained which has the lowest energy. This is a challenging task and it would be nearly impossible to explore all the electronic and ionic configurations that may be possible for a given number of atoms in a cluster except in the case where this number is restricted to a few atoms. Though much progress has been made by the steepest descent root, the energy surface is in general very complicated for most systems and in such situations other strategies based on simulated annealing become more efficient.

2.1.2 The molecular dynamics approach

The development of the ab-initio molecular dynamics method[23] has provided an efficient way for the optimization of the energy functional with respect to the electronic and ionic degrees of freedom *simultaneously*. This method relies on the assumptions that the ions can be regarded as classical particles and that the motion of the electrons and the ions can be treated within the Born-Oppenheimer(BO) approximation. The ab-initio MD exploits the fact that in the BO approximation the electrons follow the ions *instantaneously* as they move and therefore remain very close to the ground state of the corresponding ionic configuration. This eliminates the need to find the electronic ground state for each ionic configuration and therefore reduces the computaional effort very significantly.

In the MD approach the electronic $\{\psi_i\}$ and the ionic $\{\mathbf{R}_I\}$ degrees of freedom in the energy functional $E[\{\psi_i\},\{\mathbf{R}_I\}]$ are taken to be time dependent and a Lagrangian is introduced :

$$L = \sum_i^{occ} f(i)\mu_i\int d\mathbf{r}|\dot{\psi}_i(\mathbf{r})|^2 + (1/2)\sum_I M_I\dot{\mathbf{R}}_I^2 - E[\{\psi_i\},\{\mathbf{R}_I\}], \quad (8)$$

which generates a dynamics for ψ_i and $\mathbf{R}_I$ through the Newton's equations of motion:

$$\mu_i \ddot{\psi}_i(\mathbf{r},t) = -H\psi_i(\mathbf{r},t) + \sum_j \Lambda_{ij}\psi_j(\mathbf{r},t) \tag{9a}$$

and

$$M_I \ddot{\mathbf{R}}_I = -\frac{\delta E}{\delta \mathbf{R}_I(t)}, \tag{9b}$$

where μ_i's are the fictitious masses for the electronic degrees of freedom which are generally taken to be independent of the state i. Λ_{ij} are the Lagrangian multipliers for the orthonormalization of the single particle orbitals ψ_i,

$$\int \psi_i^*(\mathbf{r})\psi_j(\mathbf{r})d\mathbf{r} = \delta_{ij}. \tag{10}$$

The ion dynamics described by Eq.(9) is real whereas the dynamics of the electronic degrees of freedom is fictitious and should be regarded as a means of solving the Kohn-Sham equations. For a fixed ionic configuration when the acceleration of the orbitals becomes zero, then Eq.(9a) reduces to the standard problem and the eigenvalues of the Λ matrix are the eigen values of the Kohn-Sham equations. Once the orbitals are converged, one can then use the set of Eqs.(9) to follow the coupled electronic-ionic motion. As we shall discuss later, the calculation of the forces on ions can be easily done using the Hellmann-Feynman theorem. In principle for an exact calculation of the Hellmann-Feynman forces the electrons should be in the ground state at any instant of time during the simulation. This can be done but it is computationally very expensive. In the CP method, however, the dynamical simulation can be performed accurately (within a certain bound) when the deviation from the BO surface is small. This is due to a cancellation of errors in the calculation of the Hellmann-Feynman forces as the electron- ion dynamics proceeds. This cancellation follows from the fact that plasma frequencies are generally much higher than the ionic frequencies. Therefore during a period of the ionic motion the orbitals would oscillate several times around the ions. The forces exerted on the ions by the electrons due to deviation from the BO surface would oscillate around the correct value and would be nearly cancelled when averaged over several oscillations. Therefore for a successful CP dynamics the smallest plasma frequency should be larger than the largest ionic frequency. Further, the energy gap between the highest occupied and the first excited state in the electronic energy spectrum should be larger than the thermal energy associated with the ionic motion (see also the chapter by Pastore in this volume). This is typically the case for semiconductors and insulators. In such cases, for a given temperature there is very little transfer of energy between the ions and the electrons for a significant and in some cases even for the whole observation time of the simulation and the electrons remain very close to the BO surface. However, in metals the energy gap between the highest occupied and the lowest unoccupied states is zero and therefore it becomes a problem to keep the electrons moving adiabatically. As the simulation proceeds the kinetic energy associated with the electronic degrees of freedom increases at the expense of the

kinetic energy of the ions. In such situations one should ,in principle, use[55] the fractional occupation of various states according to the Fermi-Dirac distribution function at any finite temperature. An easy way to overcome this problem is to bring the electrons close to the instantaneous ground state after a certain number of time steps and then proceed with the simulation again. This would generally lead to a cooling of the ions. To avoid this problem Nose[56] thermostat has been used to keep the ionic temperature at a desired value. This, however, does not eliminate the problem of energy transfer to electrons. Blöchl and Parrinello[57] have used a Nose thermostat for the electrons also so that the electrons remain close to their ground state. However, such constraints increase the computational effort significantly. For clusters as the electronic energy spectrum is discrete, the condition of large gap between the highest occupied molecular orbital (HOMO) and the lowest unoccupied molecular orbital (LUMO) is satisfied in some cases (in particular for the magic clusters) whereas for other clusters and more so for larger clusters of metals, deviation from adiabatic behaviour could be significant to warrant frequent electron minimization or adopt other strategies. The formulation presented here is general and can be applied to solids, liquids or finite systems.

2.2 Implimentation of molecular dynamics using pseudopotentials

In the foregoing discussion we did not assume any particular form of ionic potential. Though there have been interesting developments of doing all electron[58] MD simulations, most studies have been done using pseudopotentials[59] which allow the use of a plane wave basis set. A plane wave basis is convinient particularly when the ions have to be moved as the plane waves are not localized on a particular site. Then the wavefunction in (1) can be written as

$$\psi_i^{\mathbf{k}}(\mathbf{r}) = \sum_{\mathbf{G}} C_{\mathbf{G}}^{\mathbf{k}} exp[i(\mathbf{k}+\mathbf{G}).\mathbf{r}]. \tag{11}$$

The sum over G is usually truncated to include plane waves upto a certain kinetic energy which determines the accuracy of the calculation. Further, the use of plane waves assumes imposition of periodic boundary conditions which are also used in classical MD simulations in bulk systems. In the case of clusters, the MD cell is taken to be sufficiently large so that the interaction between the cluster and its periodic images is negligible. k is a wave vector in the Brillouin zone. For achieving self-consistency one generally uses a set of a few special k points[60]. However, in the case of clusters, as the cell dimensions are large, one can use just a single k point , the Γ point, in (11) to sample the Brillouin zone of the MD supercell and neglect the band dispersion. This has an additional advantage that the single particle orbitals become real and therefore the computational effort reduces significantly. Henceforth, we shall drop the k index.

The total potential from the ions can be written as

$$V_{ext}(\mathbf{r}) = \sum_I v^I_{ps}(\mathbf{r} - \mathbf{R}_I). \tag{12}$$

where $v^I_{ps}(\mathbf{r})$ is the pseudopotential for the I^{th} ion. There are several ionic pseudopotentials available in the literature[61,62]. However, in most applications norm-conserving pseudopotentials of Bachelet *et al*[61] have been used as these have been tabulated. In general, we can write the ionic pseudopotential as,

$$v^I_{ps}(\mathbf{r}) = \sum_{l=0}^{\infty} v^I_l(r)\hat{P}_l. \tag{13}$$

$\hat{P}_l$ is the angular momentum projection operator which projects out the l^{th} angular momentum component of a function. $v^I_l(\mathbf{r})$ is the pseudopotential which operates on the l^{th} angular momentum component of the wave function. If one assumes $v^I_l = v^I_{l_{max}}$ for $l \geq l_{max}$ then the infinite sum in (13) can be rewritten as

$$v^I_{ps}(\mathbf{r}) = v^I_{l_{max}}(r) + \sum_{l=0}^{l_{max}-1} \Delta v^I_l(r)\hat{P}_l, \tag{14}$$

where

$$\Delta v^I_l(r) = v^I_l(r) - v^I_{l_{max}}(r). \tag{15}$$

$v^I_{l_{max}}$ is local and therefore Δv^I_l becomes the non-local part of the ionic pseudopotential. Thus we can write the total ionic potential as a sum of a local contribution, $V_{loc}(\mathbf{r})$ and a non-local contribution, $\Delta V_{nl}(\mathbf{r})$.

In the MD approach for solving the Kohn-Sham equations the expansion coefficients become time dependent and therefore the equation of motion for ψ_i can be recast into equation of motion for $C_{\mathbf{G}}$. Substituting Eq.(11) in (9a) and multiplying with $exp(-i\mathbf{G}'.\mathbf{r})$ and integrating over $\mathbf{r}$ gives

$$\mu_i \ddot{C}_{\mathbf{G}} = \sum_{\mathbf{G}'}[1/2|\mathbf{G}|^2\delta_{\mathbf{G}\mathbf{G}'} + V_{loc}(\mathbf{G}-\mathbf{G}') + \Delta V_{nl}(\mathbf{G},\mathbf{G}') + V_H(\mathbf{G}-\mathbf{G}') + V_{xc}(\mathbf{G}-\mathbf{G}')]C_{\mathbf{G}'} + \sum_j \Lambda_{ij}C^j_{\mathbf{G}}. \tag{16}$$

These equations are then numerically integrated using the standard MD procedures such as Verlet algorithm or the conjugate gradient technique. In the Verlet algorithm, the second derivative is written as a second order difference equation:

$$C_{\mathbf{G}}(t+\Delta t) = 2C_{\mathbf{G}}(t) - C_{\mathbf{G}}(t-\Delta t) + \Delta t^2 \ddot{C}_{\mathbf{G}}(t). \tag{17}$$

It introduces an error of order $(\Delta t)^4$ into the integration of the equations of motion. A more sofisticated finite difference equation could also be used but this

would require storing the coefficients for a larger number of time steps and since these are large arrays, the storage can become a problem.

2.2.1 Electron minimization

The simulation proceeds with an initial choice of the ionic distribution and of the coefficients in the expansion of the wave functions which are orthonormalized. The latter can be used to construct the charge density $n_e(\mathbf{r})$ and therefore the exchange correlation potential and energy. The Hartree contribution to potential is easily calculated by performing a fast Fourier transform (FFT) of $n_e(\mathbf{r})$ and it is given by

$$V_H(\mathbf{G}) = 4\pi n_e(\mathbf{G})/G^2. \tag{18}$$

The local contribution to the total ionic potential $V_{loc}(\mathbf{G})$ is

$$V_{loc}(\mathbf{G}) = \sum_\alpha S_\alpha(\mathbf{G})v^\alpha_{loc}(\mathbf{G}), \tag{19}$$

where S_α is the structure factor for the specie α and is given by

$$S_\alpha(\mathbf{G}) = \sum_p exp(i\mathbf{G}.\tau^\alpha_p). \tag{20}$$

Here τ^α_p is the position of the p^{th} atom of type α in the basis. The sum over p is on all the atoms of type α and

$$v^\alpha_{loc}(\mathbf{G}) = \frac{1}{\Omega_e}\int d\mathbf{r} v^\alpha_{loc}(r)exp(i\mathbf{G}.\mathbf{r}), \tag{21}$$

where Ω_e is the cell volume. The Hartree and the local ionic potential terms can now be transformed into real space with a fast Fourier transform to construct, together with $V_{xc}(\mathbf{r})$, the product $V(\mathbf{r})\psi(\mathbf{r})$ whose transform leads to the convolutions in Eq.(16). The non-local contribution needs separate attention as it is not in the form of a convolution. The non-local contribution to potential is

$$v^I_{nl}(\mathbf{G},\mathbf{G}') = 4\pi \sum_{l=0}^{l_{max}-1}(2l+1)P_l(cos(\theta_{\mathbf{G}\mathbf{G}'}))\int d\mathbf{r} r^2 j_l(Gr)j_l(G'r)\Delta v^I_l(r). \tag{22}$$

Here P_l is the Legendre polynomial of order l and j_l is the spherical Bessel function of the first kind of order l. $\theta_{\mathbf{G}\mathbf{G}'}$ is the angle between $\mathbf{G}$ and $\mathbf{G}'$. Evaluation of E_{nl} would require computation of $N_s N N_p(N_p+1)/2$ integrals where N_s and N_p are respectively the number of states and the plane waves. This is a very time consuming operation due to large values of N_p. It can, however, be simplified following a suggestion from Kleinmann and Bylander[63] who transformed the semi non-local part of the potential (local in radial part but non-local in angular part) into a fully non-local operator:

$$\Delta v_{nl}^{\alpha KB} = \sum_{l,m} \frac{|\Delta v_l^\alpha(r)\Phi_{l,m}^\alpha| >< \Phi_{l,m}^\alpha|\Delta v_l^\alpha(r)|}{< \Phi_{l,m}^\alpha|\Delta v_l^\alpha|\Phi_{l,m}^\alpha >}. \quad (23)$$

Here $\Phi_{l,m}^\alpha$ is the atomic pseudo wavefunction for specie α. It can easily be varified that in the case of atom, the fully non-local and the semi non-local forms lead to the same solution. However, the same is not true when this separable form is used in other situations. In particular ghost states have been found[64] in some cases. This can ,however, be taken care of by a suitable choice of the local potential. With this choice, the Fourier components of the non-local pseudopotential can be written into a separable form such that

$$v_{nl}(\mathbf{G},\mathbf{G}') = \sum_{l=0}^{l_{max}-1} F_l(\mathbf{G})F_l(\mathbf{G}'), \quad (24)$$

where F_l and $F_{l'}$ are functions of only one wave vector. This reduces the number of integrals to $N_s N N_p$.

2.2.2 Total energy and forces on ions

The total energy[65] can be written as

$$E = E_{KE} + E_H + E_{ps} + E_{xc} + E_{ion}. \quad (25)$$

The kinetic energy of electrons and the Hartree term are given by

$$E_{KE} = (1/2)\sum_{i,\mathbf{G}} f(i)\mathbf{G}^2 C_{\mathbf{G}}^* C_{\mathbf{G}}, \quad (26)$$

and

$$E_H = \frac{1}{2}\sum_{\mathbf{G}}{}' V_H(\mathbf{G})n_e(-\mathbf{G}). \quad (27)$$

The prime indicates that the $\mathbf{G} = 0$ term is excluded in the summation. This represents the long range slowly varying part of the Coulomb potential. For a neutral system, the *total* contribution to energy from $\mathbf{G} = 0$ term is zero in the case of a purely $1/r$ potential. However, since we are using pseudopotentials, there is a non-zero contribution coming from these terms and it needs to be treated carefully. It is convinient to smear the ion core charge into a Gaussian[66] given by

$$n_c^I(\mathbf{r} - \mathbf{R}_I) = \frac{Z_I}{(R_I^c)^3}\pi^{-3/2} exp(-|\mathbf{r} - \mathbf{R}_I|^2/(R_I^c)^2), \quad (28)$$

where R_I^c is the width of the Gaussian. The potential felt by an electron due to this distribution is

$$v_c(\mathbf{r} - \mathbf{R}_I) = -\frac{Z_I}{|\mathbf{r} - \mathbf{R}_I|} erf(|\mathbf{r} - \mathbf{R}_I|/R_I^c). \quad (29)$$

The total charge distribution and potential from the Gaussian smeared ion-cores are,

$$n_c(\mathbf{r}) = \sum_I n_c^I(\mathbf{r} - \mathbf{R}_I),$$

and

$$V_c(\mathbf{r}) = \sum_I v_c(\mathbf{r} - \mathbf{R}_I). \quad (30)$$

Considering the electronic and ionic charge distributions together as a neutral system, the Hartree, the local pseudopotential and the Madelung (E_{ion}) terms can be written together as

$$E_H + E_{ps}^{loc} + E_{ion} = \frac{1}{2}\int d\mathbf{r}d\mathbf{r}' \frac{n(\mathbf{r})n(\mathbf{r}')}{|\mathbf{r} - \mathbf{r}'|} + \int d\mathbf{r} n_e(\mathbf{r}) \sum_I w_{loc}(|\mathbf{r} - \mathbf{R}_I|) - E_{self} + \Delta_c. \quad (31)$$

where $n = n_e + n_c$ and

$$w_{loc}(r) = [v_{l_{max}}^I(r) + \frac{Z_I}{r} erf(r/R_I^c)]. \quad (32)$$

The second term in the above equation arises from Gaussian smeared ion cores (Eq. 29) and should be subtracted as it has been included in the first term on the right hand side of Eq.(31). The latter can now be evaluated in the Fourier space and is given by,

$$\frac{1}{2}\sum_{\mathbf{G}} n(\mathbf{G})^* n(\mathbf{G}) 4\pi/G^2, \quad (33)$$

where,

$$n(\mathbf{G}) = n_e(\mathbf{G}) + \sum_\alpha S_\alpha(\mathbf{G}) n_c^\alpha(\mathbf{G}), \quad (34)$$

and $n_c^\alpha(\mathbf{G})$ is the Fourier transform of the smeared ion-core charge of the α specie. Therefore, the explicit evaluation of the Madelung sums is avoided. w_{loc} is a short range potential as the long range parts of the two terms in Eq. (32) cancel each other. E_{self} is the self-interaction of the Gaussian smeared ion core charges which is included in the first term in Eq. (31) and should be subtracted. Δ_c is a correction to the first term in Eq. (31). It is equal to the difference in the interaction between the original point charges Z_I and the Gaussian broadened charges. These are given by,

$$E_{self} = 1/2 \sum_I{}' \int d\mathbf{r}d\mathbf{r}' \frac{n_c^I(\mathbf{r} - \mathbf{R}_I)n_c^I(\mathbf{r}' - \mathbf{R}_I)}{|\mathbf{r} - \mathbf{r}'|}$$

which from Eq.(28) simplifies to

$$\frac{1}{\sqrt{(2\pi)}}\sum_I \frac{Z_I^2}{R_I^c}. \tag{35}$$

and

$$\Delta_c = 1/2\sum_{I\neq J}\{\frac{Z_I Z_J}{|\mathbf{R}_I-\mathbf{R}_J|} - \int d\mathbf{r}d\mathbf{r}'\frac{n_c^I(\mathbf{r}-\mathbf{R}_I)n_c^J(\mathbf{r}'-\mathbf{R}_J)}{|\mathbf{r}-\mathbf{r}'|}\}$$

which reduces to

$$1/2\sum_{I\neq J}\frac{Z_I Z_J}{R_{IJ}}erfc(\frac{R_{IJ}}{R_{IJ}^c}), \tag{36}$$

where $R_{IJ} = |\mathbf{R}_I - \mathbf{R}_J|$ and $R_{IJ}^c = \sqrt{(R_I^{c2} + R_J^{c2})}$.

The remaining contribution to the total energy comes from the non-local part of the pseudopotential and it is given by

$$E_{nl} = \sum_i f(i)\sum_I \sum_{\mathbf{G},\mathbf{G}'} e^{-i\mathbf{G}.\mathbf{R}_I} C_{\mathbf{G}}^* v_{nl}(\mathbf{G},\mathbf{G}') e^{i\mathbf{G}'.\mathbf{R}_I} C_{\mathbf{G}'}, \tag{37}$$

whereas the exchange correlation energy can be calculated from Eq. (6).

The forces on ions can be calculated from Eq. (7) following the Hellmann-Feynman theorem according to which it is sufficient to know the changes in the Hamiltonian when the ions move, the contribution from the changes in the wavefunction being zero. The $\mathbf{R}_I$ dependent term in the Hamiltonian is the electron-ion interaction. The other contribution to force would come from the Madelung energy. From the above reformulation of the various contributions to the total energy, it can be noted that the contributions would come from Eq.(33), w_{loc}, Δ_c and E_{nl}. These can be written as,

$$\sum_{\mathbf{G}}[n^*(\mathbf{G})n_c^I(\mathbf{G})4\pi/G^2 + n_e^*(\mathbf{G})w_{loc}(\mathbf{G})](iG)e^{i\mathbf{G}.\mathbf{R}_I} + \frac{\partial\Delta_c}{\partial\mathbf{R}_I} + \frac{\partial E_{nl}}{\partial\mathbf{R}_I}, \tag{38}$$

where,

$$\frac{\partial\Delta_c}{\partial\mathbf{R}_I} = \sum_J{}'[(-)Z_I Z_J\frac{\mathbf{R}_{IJ}}{R_{IJ}^3}erfc(\frac{R_{IJ}}{R_{IJ}^c}) + \frac{Z_I Z_J}{R_{IJ}R_{IJ}^c}\frac{2}{\sqrt{\pi}}e^{-(R_{IJ}/R_{IJ}^c)^2}], \tag{39}$$

and

$$\frac{\partial E_{nl}}{\partial\mathbf{R}_I} = 2\sum_{ij} f(i)\Re(\frac{\partial W_{ij}^*}{\partial\mathbf{R}_I}W_{ij}), \tag{40}$$

with

$$W_{ij} = \sum_{\mathbf{G}} C_{\mathbf{G}}^* F_i(\mathbf{G}) e^{i\mathbf{G}.\mathbf{R}_I}. \tag{41}$$

The prime in Eq. (39) indicates that $J = I$ term is excluded.

2.2.3 Orthogonalization of wave functions

After the forces are calculated, the set of Eqs. (9) have to be solved with the constraints (10). Starting with a set of orthonormalized ψ_i, the parameters Λ_{ij} can be calculated[46] by differentiating (10) twice and using (9a), to obtain:

$$\Lambda_{ij} = <\psi_j(\mathbf{r},t)|H|\psi_i(\mathbf{r},t)> -\mu\int d\mathbf{r}\dot{\psi}_j^*(\mathbf{r},t)\dot{\psi}_i(\mathbf{r},t). \tag{42}$$

Thus the Lagrangian multipliers depend upon the trajectories of the ψ_i's and therefore on the algorithm used to integrate the equations of motion. The solution of the equations of motion is achieved in two steps. First an unconstrained wavefunction $\tilde{\psi}_i$ is obtained. In the Verlet algorithm this can be written as,

$$\tilde{\psi}_i(t+\Delta t) = -\psi_i(t-\Delta t) + 2\psi_i(t) - \frac{\Delta t^2}{\mu}H\psi_i(t). \tag{43}$$

The constraint forces are then added to the wavefunctions $\tilde{\psi}_i$,

$$\psi_i(t+\Delta t) = \tilde{\psi}_i(t+\Delta t) + \sum_j x_{ij}^*\psi_j(t), \tag{44}$$

where $x_{ij}^* = (\Delta t^2/\mu)\Lambda_{ij}$. Now imposing the orthonormality condition on $\psi_i(t+\Delta t)$,

$$\int d\mathbf{r}\psi_i^*(\mathbf{r},t+\Delta t)\psi_j(\mathbf{r},t+\Delta t) = \delta_{ij}, \tag{45}$$

we get,

$$A_{ij} + \sum_k(x_{ik}^*B_{kj} + x_{jk}B_{ki}^* + \sum_l x_{ik}x_{jk}^*) = \delta_{ij}, \tag{46}$$

which can be written in matrix form as

$$\mathbf{A} + \mathbf{X}\mathbf{B} + \mathbf{B}^\dagger\mathbf{X}^\dagger + \mathbf{X}\mathbf{X}^\dagger = 1, \tag{47}$$

where, $A_{ij} = <\tilde{\psi}_i(t+\Delta t)|\tilde{\psi}_j(t+\Delta t)>$ and $B_{ij} = <\psi_i(t)|\tilde{\psi}_j(t+\Delta t)>$. Eq. (47) can be solved iteratively. Using Eq. (43) and making a Taylor series expansion of wavefunctions at time $(t-\Delta t)$, it can be shown that $A_{ij} = \delta_{ij} + \mathcal{O}(\Delta t^2)$ and $B_{ij} = \delta_{ij} + \mathcal{O}(\Delta t)$. Therefore, from Eq. (46) within second order in (Δt) we can write

$$\mathbf{X}^* = (1/2)(1-\mathbf{A}). \tag{48}$$

Then the solution to (47) can be found iteratively from

$$\mathbf{X}^{(k)} = \frac{1}{2}[1 - \mathbf{A} + \mathbf{X}^{(k-1)}(1-\mathbf{B}) + (1+\mathbf{B}^\dagger)\mathbf{X}^{(k-1)} - \mathbf{X}^{(k-1)^2}], \tag{49}$$

where k is the number of iterations. Typically it requires a few iterations to solve (47).

2.3 Simulated annealing

As the energy surface in the multidimensional configuration space is in general complicated, simulated annealing technique[67] is used to obtain the lowest energy structures. In this technique the cluster is heated upto a certain temperature T so that the ions start diffusing. This temperature is in general different for different materials and will in general also differ for different clusters of a material as the binding energy per atom may change significantly with cluster size. The cluster is then allowed to evolve at this temperature for a few pico-seconds which is a rather short time as compared to standard classical molecular dynamics simulations where the observation time is of the order of nano-seconds. Experience with different systems has, however, shown that this period is sufficient to make the cluster loose completely the memory of its starting configuration. Subsequently it is then cooled such that the system remains close to the BO surface. The time step for integration of the equations of motion is taken to be such that there is negligible transfer of energy from the ionic to the electronic degrees of freedom. As discussed above, in the case of clusters having a large HOMO-LUMO gap it has been found that the system can remain close to the BO surface even for the whole period of the simulation. The simulated annealing procedure has proved very successful in finding new structures which have lower energy than the lowest energy structures obtained by other methods in some cases. Also it provides a natural way to study the dynamical properties of clusters and the changes in the atomic and electronic structure at finite temperatures which are going to be important in understanding reactions on clusters. In the next section we discusss some of the systems to which this technique has been successfully applied.

3. Applications to clusters

3.1 Clusters of metals

In their pioneering experiments on simple metal clusters, Knight *et al*[68] observed marked stability of sodium clusters with 8, 20, 40, 58, and 92 ... atoms (Fig. 2a). Sodium has one valence electron and therefore clusters with 8, 20, 40, 58 and 92 ... valence electrons are particularly abundant. Such clusters are referred to as *magic* clusters as the abundance of clusters having one more atom is significantly less. Similar results have been obtained for clusters of other alkali metals[69] and their mixed clusters[70] as well as clusters of noble[71] metals. Clusters of divalent[72] elements also show marked stability for the same number of valence electrons. However, small clusters of divalent elements are weakly bonded due to the ns^2 closed shell configuration. Therefore, as the cluster size increases, there occurs a non-metal - metal transition which we shall discuss in detail later. Studies of the ionization

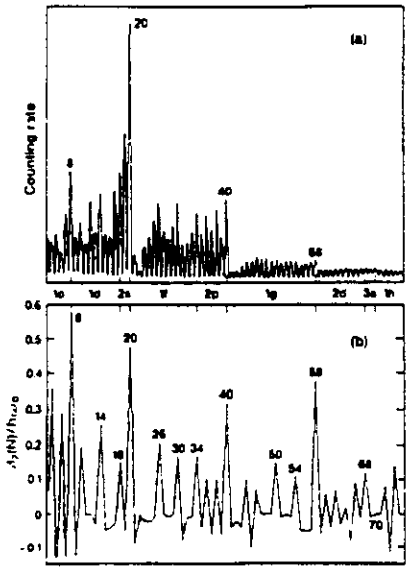

Figure 2: (a) Abundance spectrum of sodium clusters and (b) the second order derivative of energy calculated within an ellipsoidal modified harmonic oscillator model. (After Clemenger[81])

potentials[73], fragmentation[74] and polarizabilities[75] of metal clusters and reactions of some gases with them[19,20] have provided further information about their stability and electronic structure.

While experimental studies have been carried out on clusters of several metals, ab-initio MD method has been applied mainly to clusters of $s-p$ bonded metals such as Na, K, Be, Mg, Al, Sn, and binary clusters of Na-K , Na-Mg as well as doped clusters of Al. Calculations have also been performed on dimers of group IB and IIB elements[76] and clusters of semi-metals Sb[33,34] and Ga[37,38]. These studies have provided information about the low lying structures, bonding nature and dynamics of clusters. Before these calculations became possible, the spherical jellium model[22,77] (SJM) played the central role in the study of metal clusters and it is still a nice model to understand many of the results obtained by these elaborate

calculations. We therefore first describe the essential results of this model.

3.1.1 The jellium model

Alkali and other simple metals are quite well described by a nearly free electron model as the effective ionic (pseudo-) potential seen by the valence electrons is nearly constant throughout the metal. The weak pseudopotential can be approximately treated as a perturbation on the free electron like behaviour of the $s-p$ conduction electrons in these metals. The same features can be expected to hold for clusters of these elements. However, as the structure of clusters is not known in most cases, one can consider a cluster to be spherical in the lowest approximation and solve the problem of electrons in a spherical potential well. Thus Knight and coworkers[68] used a simple spherical potential to study the stability of clusters as a function of the number of valence electrons. Very similar to the shell structure in atomic spectrum[78] as well as in nuclear physics[79] they correlated the stability of clusters with the filling of the electronic shells 1s, 1p, 1d, 2s, 1f, 2p, 1g, ... in the spherical potential. Later, Cohen and collaborators[22,60] used SJM in which the ionic spherical potential. Later, Cohen and collaborators[22,60] used SJM in which the ionic charges were smeared out in a uniform positive spherical background such that

$$n_+(r) = \begin{cases} n_0 & \text{if } r < R \\ 0 & \text{otherwise} \end{cases} \quad ; \tag{50}$$

Here R is the radius of the cluster which is related to the number of atoms N in the cluster.

$$\frac{4}{3}\pi R^3 = N\Omega, \tag{51}$$

where Ω is the volume per atom in the macroscopic metal. The constant positive density n_0 is related to Ω and the number of valence electrons Z (the subscript I is dropped as only one type of atoms are considered) by $Z = n_0\Omega$. The Kohn-Sham equations (1) are then solved to obtain the eigenvalues and the total energies. Similar to the spherical potential model the energy levels of the electrons are again characterized by the radial and angular quantum numbers. The 1s, 1p, 1d, 2s, 1f, 2p, 1g, 2d, 3s, 1h, ... shells are respectively filled for the total valence electron numbers, 2, 8, 18, 20, 34, 40, 58, 68, 70, 92, and so on in the cluster. The closed shell configurations are stable due to energy gaps between electronic shells and again this simple model provides a good explanation for the marked stability observed in alkali metal clusters for 8, 20, 40, 58 and 92 atoms. The fine structure in the abundance spectrum can be understood in terms of the completion of the subshells that arise due to deformation of the spherical positive background. Clemenger[81] has studied the effects of the ellipsoidal deformations on a three dimensional modified harmonic oscillator model. As shown in Fig. 2b this deformation leads to fine structure in the second order energy difference, Δ_2 which shows peaks at $N = 10, 14, 18, 26, 30, 34, 36, 38, 44, 46, 54$ etc. corresponding to subshell filling in addition to the main peaks at $8, 20, 40, 58, \ldots$ For shell closing numbers not

observed in the experiment the reason may be that only a large gap to the next shell enhances the stability of a closed shell or the SJM is not a good representation of the actual potential seen by the electrons in a cluster. The nucleation conditions can also affect the abundance spectrum. The absence of fine structure in the abundance spectrum for large clusters is due to smaller gaps for higher shells while the variation in the intensities of clusters of different elements in the same group is possibly due to the difference in the kinetic behaviour and different ionic potentials. While the general trends in several properties such as relative stability, ionization potential, polarizability etc. of metal clusters are well described[22,77] by the jellium model and it has the advantage of being applicable easily to large clusters containing several hundred atoms, it is of interest to study these aspects from a more realistic model and to understand their atomic structure and dynamical properties. In the following we review results on clusters of several systems obtained by using the ab-initio molecular dynamics method.

3.1.2 Alkali metal clusters

Several theoretical studies have been made on clusters of alkali metals but sodium is one of the most extensively studied. Ballone *et al*[28] studied Na_8, and $Na_{10}K_{10}$ clusters. More recently a very detailed LDA study on sodium clusters having upto 20 atoms has been carried out by Röthlisberger and Andreoni[29]. Several interesting observations have been made. First of all when the results of these calculations are analysed in terms of the angular character of the electronic states around the center of mass of the cluster, then the low temperature electronic structure agrees with the predictions of the shell model. However, one finds that with increasing temperature the clusters become less and less spherical and the hybridization between states of different angular momentum increases due to the decrease of energy gaps. This is in contrast to the widely held belief that the clusters tend to be spherical as the temperature increases and that the validity of the jellium model is enhanced in warm clusters. The hybridization is less pronounced for magic clusters but increases with increasing size due to the decrease in the spacing between the one-electron energy levels.

The potential energy surface is found to be rather flat and the electronic charge density, delocalized. However, there is a preference for pentagonal rings analogous to the complexes of Lennard-Jones systems. The energy difference between several low-energy structures is tiny. But even in this case the SA has proved very useful as a powerful optimization technique. The small energy differences for various cluster structures are also in agreement with the results in bulk where accurate LDA calculations[82] predict a difference of 2 meV between hcp and bcc and 3.5 meV between hcp and fcc structures.

The non-magic clusters such as Na_{10} and Na_{13} tend to have many more isomers which are nearly degenerate with the lowest energy structure, as compared to the magic clusters such as Na_8 and Na_{70}. The lowest energy structure of Na_8 is found to be dodecahedron which has the D_{2d} symmetry. This is nearly degenerate

with the one having the T_d symmetry which was predicted to be the lowest energy structure from configuration interaction calculations[83].

Fig. 3 shows four structures for Na_{20} cluster. (a) and (b) have been obtained from simulated annealing and are nearly degenerate. These are based on pentagonal motif. Interestingly (b) is also the ground state and (a) a local minimum for Lennard-Jones clusters. (c) and (d) have tetrahedral symmetry. In this case the electronic states can be classified with good accuracy by their angular momentum in agreement with the shell model. However, in contrast to the Na_8 cluster, Na_{20} looses this shell model character even at as low temperatures as 200 K. Accordingly 8-atom clusters are predicted to be more stable with respect to increasing temperature. In fact the diffusion coefficient was estimated to be 0.5×10^{-4} cm^2/sec for Na_{20} at 640 K from the root mean square displacement and it is only a factor of 3 lower than the value for liquid sodium at the same temperature. Further, the electronic structure is found not to be very sensitive to the atomic structure and therefore the electronic properties may not be useful as a probe to study the structure. In Fig. 4 we have shown the spherical average of the electronic charge density around the center of the cluster corresponding to four isomers shown in Fig. 3. One can see that there is very little variation from one structure to another beyond the core region. However, the vibrational spectra has been found to show a stronger dependence on structure and can be used as a probe to get some information about the structure.

For non-magic clusters such as Na_{10}, one can consider the cluster to be made up of a core which is more rigid and some cap ions which are constantly farther away from the center of the cluster. Thus individual atoms can undergo displacements larger than the typical interatomic distance. As shown in Fig. 5, the displacement of cap ions is far more than for those in the core region. However, the radial movement is much smaller than the root mean square displacement which indicates that the cap ions travel more on the surface of the cluster. While such a detailed study is not available for clusters of other alkali metals, we expect to have similar behaviour for them as also indicated from results of a few other studies and those in the bulk. In fact calculations[84] on Cs clusters do show that the general trends remain the same though the energy differences between different isomers become even smaller than in the case of Na.

Very recently Fois *et al*[85] have done a LSD study of Na clusters and have also studied the effect of the self-interaction correction (SIC). While for Na_6 the LSD calculation predicts the same structure as obtained from the LDA calculation, namely a pentagonal pyramid to be lower in energy than a 2-dimensional triangular structure, in the LSD-SIC calculation the triangular structure has a lower energy than the pentagonal pyramid. These results no doubt raise the question of the correctness of the LDA/LSD geometries. However, we expect that the trends and the information about the dynamics and the charge densities obtained from the LDA/LSD calculations are useful in understanding the general behaviour of clusters of differet sizes.

Mixed clusters of Na and K have also been studied within LDA and a ten-

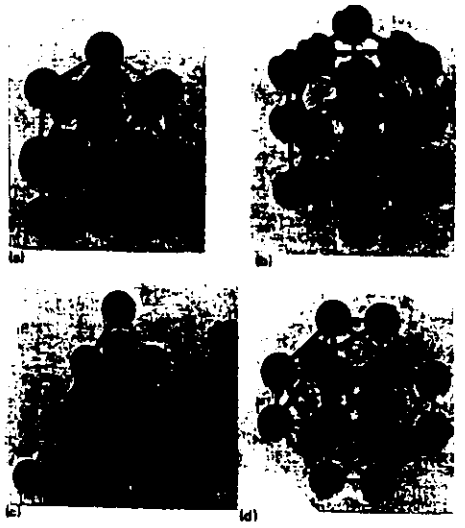

Figure 3: Isomers of Na_{20}. (a) and (b) are lowest energy structures whereas (c) and (d) are higher energy structures of T_d symmetry. (After Röthlisberger and Andreoni[29])

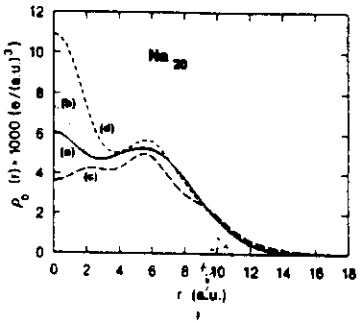

Figure 4: Spherical average of the electron density (here denoted by ρ_0) in the four structures of Fig. 3 for Na_{20}. r = 0 corresponds to the center of the cluster. (After Röthlisberger and Andreoni[29]).

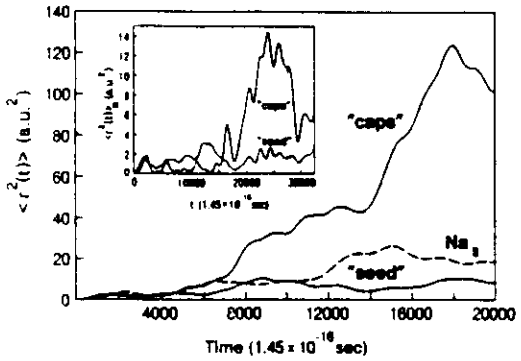

Figure 5: Time variation of the mean square displacement of 'caps' and 'seed' ions for Na_{10} cluster at 260 K. The inset shows the radial part. Note the difference between the scale of the main plot and the inset. For comparison the mean square displacement of the atoms in Na_8 around the same temperature is also shown by dashed line. (After Röthlisberger and Andreoni[29])

dency for K segregation on the surface has been found[28]. This is expected also on the basis of simple models based on broken bonds on a surface and the atomic size mismatch. According to these models, the element having the lower surface energy (larger size) tend to segregate at the surface[86]. This segregation might lead to preferential evaporation of the larger specie and favour clusters enriched with smaller atoms. The lowest energy structure of this mixed cluster is similar to that of Na_{20} and the one - electron orbitals are delocalized over the entire cluster. In agreement with the experimental observations[70], the shell model behaviour is applicable to this alloy in spite of the ionic segregation. Also for Mg doped Na_N clusters a tendency for Mg ion segregating to the surface has been obtained[44]. However, in this case due to surface segregation there is hybridization between states of different angular momentum components and the shell model is not quite applicable. On the other hand when a small size atom is doped as in the case of Na_7Al cluster, then the impurity ion prefers to sit inside the cluster and the electronic structure agrees with the predictions of the jellium model.

The finite temperature studies of clusters provide useful information about their dynamical behaviour. The vibrational spectrum (Fig. 6) of Na_7Mg cluster has a soft 'diffusive' mode as well as a high frequency mode, the latter being absent in pure sodium clusters. Even at 100 K a sodium atom which caps a pentagonal pyramid (Fig. 6) diffuses around the fivefold axis and gives rise to the soft mode. Whereas the high frquency mode corresponds to a strong bond between Na and Mg atoms which also causes Mg to have a high coordination with Na atoms.

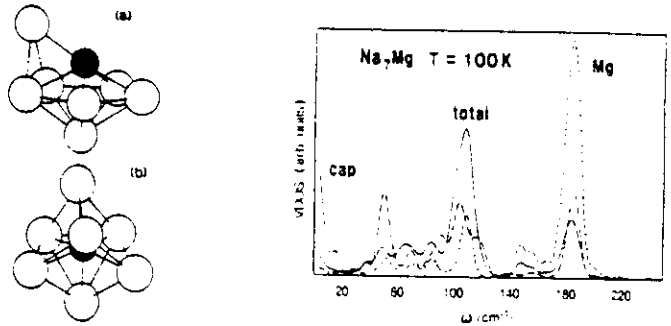

Figure 6: Structure and the vibrational spectrum of Na_7Mg cluster. (a)lowest energy structure (pentagonal bipyramid +1) and (b) tetracapped tetrahedron which also corresponds to a low energy isomer of Na_7Al. The vibrational density of states is shown for (a) at an average temperature of 100K. Total (solid line), sodium cap (dashed line) and magnesium atom (dashed-dotted line) (After Röthlisberger and Andreoni[44]).

3.1.3 Divalent metal clusters: growth and the non-metal - metal transition

For divalent metals, extensive studies have been made recently for Mg[32,87] and Be[31] clusters. The equilibrium structures of Mg clusters having upto 13 atoms have been studied by Kumar and Car[32]. The lowest energy structures with singlet states are shown in Fig. 7. Due to a closed shell atomic electronic configuration, Mg_2 is found to be very weakly bonded with a bond length 6.33 a.u.. Experimentally Mg_2 is found[88] to have a singlet ground state with a bond length 7.35 a.u. and cohesive energy 0.027 eV/atom. The larger (smaller) value of the calculated cohesive energy (bond length) is due to the use of the LDA which over- (under-) estimates the binding energy (bond length). Ballone *et al*[89] have done a calculation with a non-local exchange correlation functional and find an improvement over the LDA results. However, the results of Kumar and Car agree very well with a LSD calculation[90] which gives 0.11 eV and 6.37 a.u. respectively for the binding energy and the bond length.

The lowest energy state for Mg_3 is an equilateral triangle with bond length 5.93 a.u.. Mg_3 chain is 0.111 eV/atom higher in energy than the equilateral triangle. Thus Mg clusters favour to maximize the coordination number. This trend is continued for bigger clusters as well. The lowest energy structure for Mg_4 is a regular

tetrahedron. This is a particularly stable cluster with considerably smaller bond length. Mg_5 is a slightly elongated trigonal bipyramid. These results are in agreement with a LSD calculation[90] which also finds a singlet state for all these clusters to be of lowest energy. These results were obtained by performing steepest descent calculations for a few selected geometries of the clusters. However, simulated annealing technique was used for larger clusters. For Mg_6 it leads to a structure shown in Fig. 7. This can be obtained by capping a face (3-4-5) of Mg_5. Independently Reuse *et al*[90] obtained an octahedron with a rectangular base to be of lowest energy for this cluster. A steepest descent calculation done by Kumar and Car[32] for this structure gives it only 0.004 eV/atom higher in energy than the simulated annealing structure, thus making them nearly degenerate. This is due to the fact that the pair distribution function for the two structures is nearly the same.

For Mg_7 the lowest energy structure is a pentagonal bipyramid. Its two apex atoms with coordination 6 have the shortest distance (5.3 a.u.) whereas the base atoms with coordination four have a bond length 6.04 a.u. As we shall discuss later, the short distance is significant from the point of view of non-metal - metal transition in these clusters. This structure can be obtained from Mg_6 by capping two faces and is also in agreement with the results obtained by Reuse et al[90] and Pacchioni et al[91] using the LSD and cofiguration interaction calculations respectively.

The lowest energy structure of Mg_8 can be simply obtained by capping a face (1-3-7) of the pentagonal bipyramid. For larger clusters a new structure starts. Mg_9 is a tricapped trigonal prism as shown in Fig. 7. This structure has some similarity with a fragment of the hcp lattice except that the bond lengths 1-4, 2-5 and 3-6 are shorter whereas for bulk Mg they correspond to the c-axis. Adding an atom to one of the triangular faces of the trigonal prism leads to the structure of Mg_{10} as shown in Fig. 7. The same result has also been obtained independently by Andreoni[34] and de Coulon *et al*[87]. This provides further confidence in SA strategy to obtain lowest energy structures. Among Mg clusters this is another most stable structure as it can be seen from the second order finite difference of the energy which is plotted in Fig. 8 along with the cohesive energy. $E(N)$ is the energy of a cluster with N atoms. While the cohesive energy increases with the size, the peaks in the difference spectrum in this plot can be correlated with the abundance in the mass spectrum. The marked stability of 4 and 10 atom clusters agree with the jellium model. Also a small peak and a shoulder appear for 7- and 9-atom clusters respectively which again agree with the fine structure in the calculated spectrum in the jellium model.

Mg_{11} is obtained by capping the other triangular face of the trigonal prism. While the eleventh atom caps the Mg_{10} cluster symmetrically, the simulated annealing results indicate it to be weakly bonded to the cluster and similar to the Na_{10} cluster, its mean square displacement is much larger as compared to other atoms in the cluster. This can cause evaporation of an atom and absence of the abundance of Mg_{11} clusters in the mass spectrum as it is generally noted. Mg_{12} is also a capped trigonal prism. However, instead of face capping, in this case an atom caps an edge of the trigonal prism.

13 atom clusters are interesting as these have been considered to have either

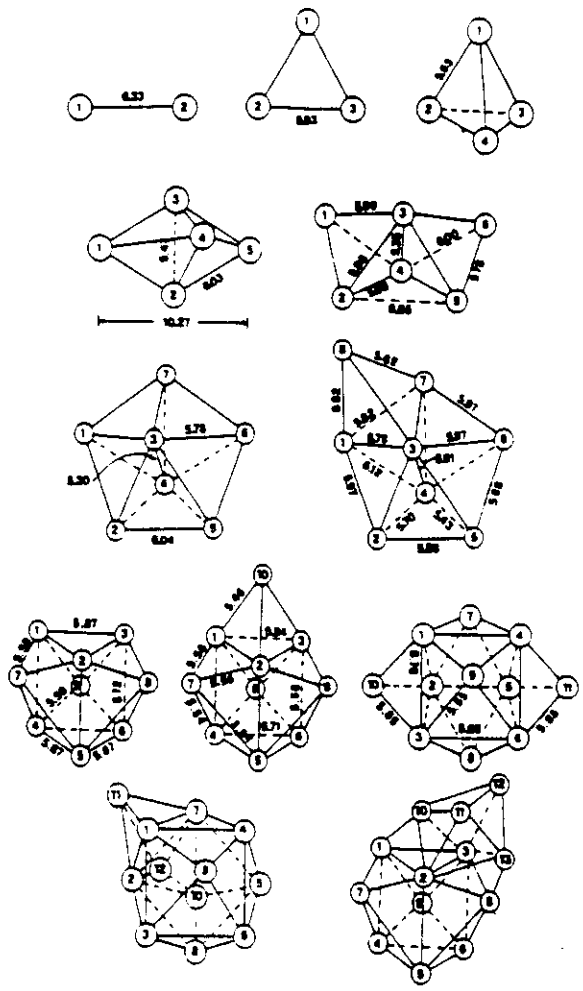

Figure 7: Lowest energy structures of Mg clusters with 2 to 13 atoms. (After Kumar and Car[32]).

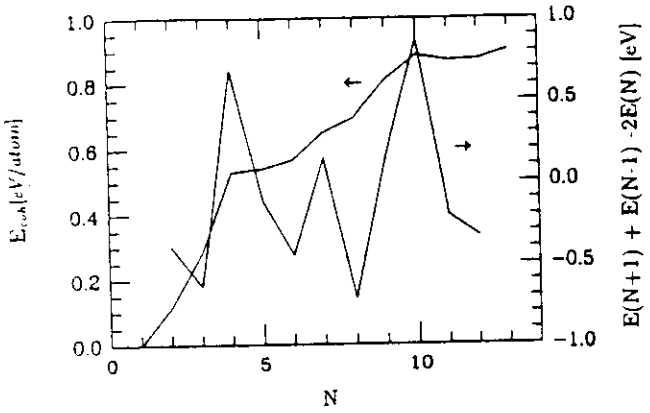

Figure 8: Plot of the cohesive energy and its second order difference spectrum as a function of the number of atoms in Mg clusters. (After Kumar and Car[32]).

an icosahedral structure which is the closest packed for 13 atoms or a cubooctahedral structure which is the closest packing in the bulk. However, Mg_{13} is neither an icosahedron nor a cuboctahedron. It can be considered to arise from the fusion of a Mg_9 and a Mg_4 cluster (atoms 10 to 13 in Fig. 7). The tetrahedron of Mg_4 opens up to form a bent distorted rhombus. Calculations[32] on Mg_4 cluster have shown that this is possible as there is no barrier for this motion. It is interesting to note that a relaxed fcc and an icosahedral structure are respectively 0.032 and 0.043 eV/atom higher in energy than the simulated annealing result. The structures themselves relax very significantly. However, relaxing a hcp cluster leads to a structure which is nearly degenerate with the one obtained from the simulated annealing. From table I it can be seen that for a 13-atom cluster the cohesive energy (see Fig. 8) is about 54% of the bulk value (1.687 eV/atom) calculated by Moruzzi *et al*[53] and much larger clusters may be needed for getting the bulk like behaviour.

An independent study of Mg clusters by de Coulon *et al*[57] also finds a tetra-capped trigonal prism for 10-atom cluster using the Car-Parrinello method. However, their results for 6-, 8-, 12- and 13- atom clusters are different from those obtained by Kumar and Car[32] and their structures lie slightly higher in energy. It may be noted that for these calculations simulated annealing was not used.

Since a non-metal - metal transition is expected for clusters of divalent elements, Kumar and Car studied the nature of bonding in these clusters by calculating the p character of charge density around various ions. Fig. 9 shows the p character obtained for different ions in a cluster. When these results are analysed together

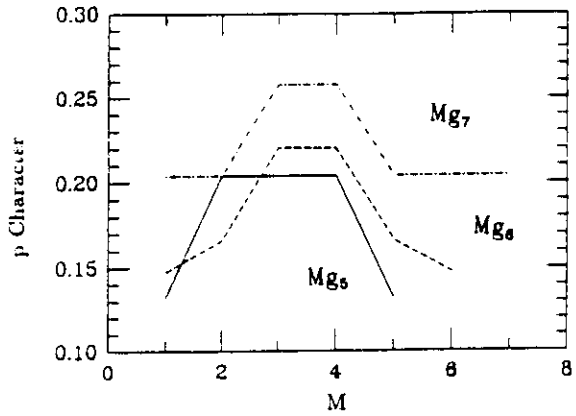

Figure 9: p character of the electronic pseudo-charge density around different ions in a few Mg clusters. Here M refers to the number of an ion as shown in Fig. 7. (After Kumar and Car[32]).

with the structure of the clusters, it is clear that the transition to metallic behaviour starts preferentially in some bonds such as bond 3-4 in Mg_7 and not in the whole cluster. Different atoms in a cluster have different p character and there are some short bonds which develop metallicity first. This is likely to be important for the study of reactivity of clusters. When the p character is averaged over the cluster, it shows an oscillatory behaviour and the convergence to the bulk value is slow. The charge density in these clusters indicate that bonding in these clusters changes slowly from weak chemical to covalent to metallic behaviour. Therefore the general agreement with the jellium model in such cases should be considered with caution.

The changes in the mean nearest neighbour bond length and the average coordination of an atom in the cluster are shown in Fig. 10. While the average coordination increases monotonically, the bond length shows an oscillatory behaviour which is suggested to be a feature of clusters showing a transition from van der Waals or weak chemical to metallic bonding. A simple reason for this is the fact that for van der Waals bonding the bond length is large and it should decrease till metallization occurs in the cluster. Beyond this there should be a tendency for the bond length to increase towards its bulk value. The sharp decrease in the bond length for 4- and 10-atom clusters is likely to be due to shell closing. This behaviour is different from clusters of metals like Cu for which the bond length has been reported to increase towards its bulk value monotonically[92].

Fig. 11 shows the chemisorption energy of Mg on Mg clusters and its correlation with the variation in the HOMO-LUMO gap. While both of these show an

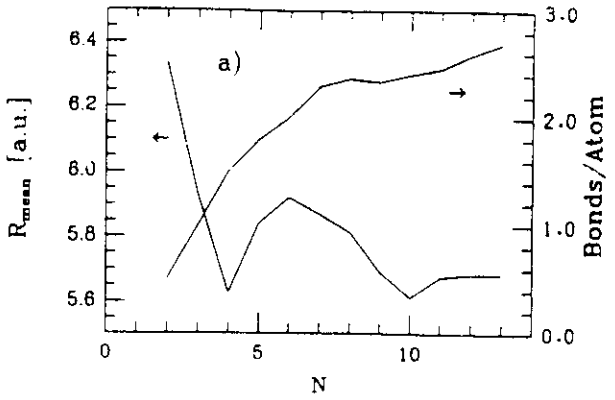

Figure 10: Mean nearest neighbour bond length (left scale) and the number of nearest neighbour bonds (right scale) as a function of the cluster size. (After Kumar and Car[32]).

oscillatory behaviour as a function of size, the magic clusters have smaller chemisorption energy and larger HOMO-LUMO gap. This is consistent with the experimental results of chemisorption of oxygen on Al clusters[20].

Kawai and Weare[31] have done a similar study for Be clusters having 2 to 20 atoms. Small clusters of Be have the same structure as for Mg. However, their calulations suggest that Be clusters tend to attain some of the features (p character) of the bulk bonding even for a 6-atom cluster whereas this is quite slow for Mg. Also Be_8 is a bicapped trigonal prism as compared to the capped pentagonal bipyramid for Mg. While Be_9 has the same structure as for Mg_9, larger clusters of Be are different and have some similarity with the bulk hcp structure. In particular, though the trigonal prism structure is retained, the capping patterns are different for the two systems. Calculations[93] for Be_{10}, a magic cluster, with the Mg_{10} structure show it to be 0.028 eV/atom higher in energy than the structure obtained by Kawai and Weare. Therefore in this size range, Be and Mg clusters have different behaviour. However, similar to Mg_{13}, for Be_{13} also, a relaxed icosahedron structure lies 0.7 eV higher in energy than the one obtained from the simulated annealing procedure. Unlike Mg clusters, there is a remarkable tendency for a two dimensional growth pattern related to hcp packing which suggests directional bonding to be very important for Be clusters and crystals. However, the orbital energies and the angular character of the wave functions for Be clusters correlate well with the predictions of the shell model described above. Also the second-order finite difference of the calculated total energy shows large maxima at N = 4, 10, and 17 which again agrees with the

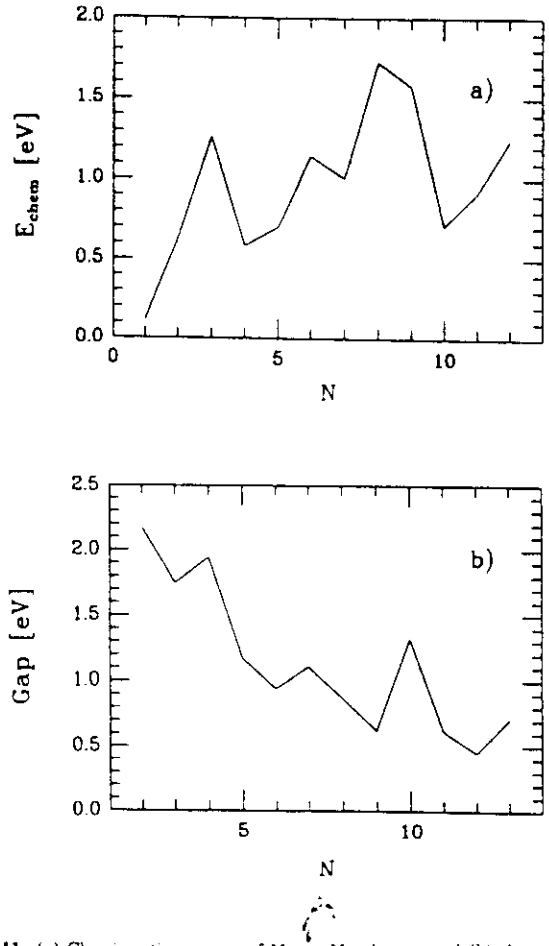

Figure 11: (a) Chemisorption energy of Mg on Mg clusters and (b) the variation of the HOMO-LUMO gap in Mg clusters. Note the correlation of small chemisorption energy with large gap. (After Kumar and Car[32]).

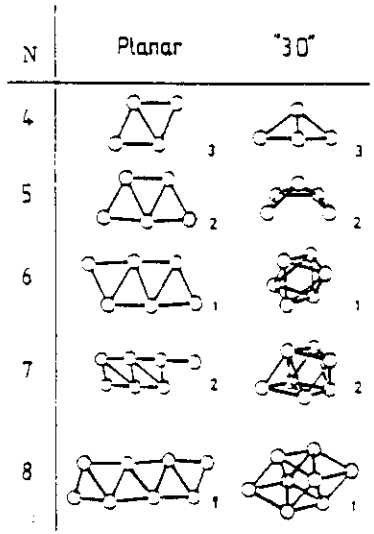

Figure 12: The structures and spin multiplicities of the most stable planar and 3-dimensional isomers of Al_N, N=4-8. Bonds are shown if the interatomic distance is less than 5.48 a.u.. The planar structure in Al_8 corresponds to a saddle point in the energy surface and buckles readily. (After Jones[36]).

shell model.

Ballone and Galli[75] studied bonding in neutral and ionized dimers of group IB and IIB metals by solving the CP equations in cylindrical coordinates and using a large cutoff of upto about 300 Ry. This large cutoff was needed because the d electrons were treated as valence electrons. As in the case of Mg_2, the binding energy and the vibrational frequency was overestimated whereas the bond length was underestimated when compared with the experimental results. It was shown that the bonding in IIB clusters could be described reasonably well by taking only the s^2 valence electrons but by incorporating the non-linear core corrections[94] and a repulsive short-range interaction with exponential shape characteristic of the closed-shell overlap due to the d-electrons. Application of the short range repulsive interaction was shown to produce the same results as obtained with very large energy cutoff for murcury dimer.

3.1.4 Trivalent metals

In this group clusters of Al and Ga have been studied in detail. Jones[36,37] has studied Al clusters having upto 10 atoms. These calculations have been done within the LSD approximation. The lowest energy structures are shown in Fig.

12 . Small Al clusters favour planar geometries. The lowest energy structure for Al_3 is an equilateral triangle while Al_4 is a rhombus with D_{2h} symmetry and is a triplet. For larger clusters three dimensional structures are favoured. The binding energy increases monotonically towards its bulk value as the cluster size increases. For Al_5 a planar C_{2v} structure is almost degenerate with a C_s structure with similar bond lengths (both doublets). For $N \geq 6$, states with minimum spin degeneracies are favored. For Al_6, the lowest lying state is (D_{3d}) and is a singlet. This is nearly degenerate with triplet D_{2d} state. Al_7^- is a nearly symmetric capping of Al_6 (D_{3d}). Al_7^+ is one of the most prominent in the mass spectrum. As it has 20 valence electrons, its stability has been correlated with the completion of the 2s shell in the spherical jellium model. For such clusters there is a large gap between the highest occupied and the lowest unoccupied orbitals. Similar behaviour was obtained by Kumar and Car for Mg_4 and Mg_{10} clusters which have 8 and 20 valence electrons respectively and are magic. Also the ionization potential of Al_7 and the dissociation energy of Al_8 are low. This is in agreement with the results for Mg_{11} cluster. In addition to these lowest energy structures, a variety of planar and buckled structures (similar to one in α - Ga) are also found to be locally stable. This is consistent with the metallic nature of Al and the fact that there are usually unoccupied orbitals near the highest occupied level and it is easy to transfer electrons between π orbitals (which dominate in the bonding in planar structures) and σ orbitals. The finding of several planar and buckled structures with arrays of triangles and having nearly the same energies can be helpful in understanding layer arrangements with triangular nets in many Al - transition metal alloys[95].

Al_{13} cluster is a classic example for studying the relative stability of icosahedral and coboctahedral structures. Negatively charged Al_{13} clusters are particularly abundant in mass spectrum[96] shown in Fig. 13. Bernholc and coworkers[36] have studied 13- atom and a few other large clusters of Al. The energy differences between the icosahedral and cuboctahedral structures for 13-, 19-, and 55- atom clusters are found to be small. For 13- atom cluster a nearly regular icosahedron is found to have the lowest energy, whereas for 55- atom cluster the structure has large distortions though its origin from an icosahedron can be discerned. While no efforts were made to make a systematic study as a function of the size, several structures were found to be close in energy for a 55- atom cluster. In the shell model of metal clusters, Al_{13} is nearly magic with 39 valence electrons and therefore a nearly perfect icosahedron has the lowest energy and a single well defined energy minimum. Adding an electron to it makes it a closed shell system which is most likely the reason for its strong abundance. On the other hand a 55- atom cluster is not magic in the shell model. The fact that several nearly degenerate structures exist for this cluster agrees also with the results of Kumar and Car[32] for Mg_{13} cluster (non-magic) in which case the structure obtained from the simulated annealing is nearly degenerate with the one obtained from relaxation of the hcp structure. However, for Al clusters the deviation from the bulk cohesive energy is not large and it was suggested that a transition from icosahedral to bulk structure may occur early.

Mixed clusters of Al have also been studied. These are interesting from

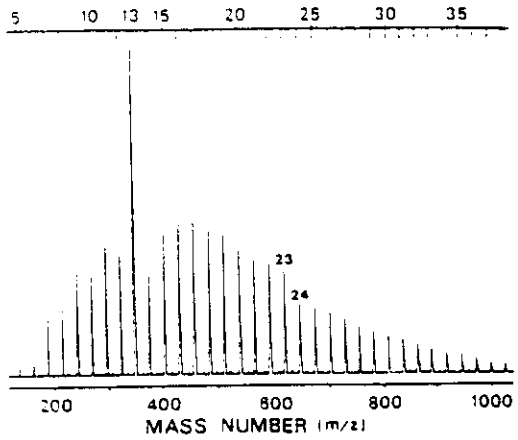

Figure 13: Time of flight mass spectrum of Al_N^- ($N = 5 - 38$) clusters. One peak at $N = 13$ and a step between $N = 23$ and 24 corresponding to magic numbers in the shell model can be observed and there are no other peakes or steps up to $N = 70$. (After Nakajima et al[96].)

several points of views. First of all there are several alloys of aluminium which have very complicated structures and in which an icosahedral unit (cluster) plays an important role. In addition, several aluminium alloys form quasicrystals in which again icosahedral order is prevalent. This together with the tendency of Al_{13} to form a nearly icosahedron merits study of the stability of such local units which may exist in crystalline, quasicrystalline or amorphous structures. Also the neutral clusters of Al do not satisfy the electronic shell closing condition. However, by suitable doping a cluster one can achieve the shell closing and enhance the stability of magic clusters of aluminium. Of particular interest are the 13 atom icosahedral clusters which may also act as entities to form new materials. Several binary clusters of aluminium have therefore been studied. Mixed clusters of Al-Mg were studied[97] using the steepest descent approach in the CP method. There are several phases of Al-Mg alloys. Among these, notable are the Frank-Kasper phase[98] in which icosahedral Al_zMg_{13-z}, $Al_{12}Mg_2$ and $Al_{12}Mg_3$ clusters are abundant. In the latter two, a Mg atom is surrounded by 12 Al and 2 or 4 Mg atoms respectively. 14 and 16 coordinated clusters were predicted by Frank and Kasper on the basis of geometrical arguments. Study of such clusters is interesting to understand the role of the electronic structure and the atomic sizes in complicated crystalline and quasicrystalline structures. For $Al_{12}Mg_2$ cluster which has 42 valence electrons, there is only a little distortion from the capped hexagonal antiprism structure found in the crystalline phases whereas for $Al_{12}Mg_3$ cluster which has 46 valence electrons,

there are considerable John-Teller distortions from the bulk atomic packing. This suggests that the bulk structure of the 17- atom cluster is not particularly stable and there are other considerations such as those suggested by Frank and Kasper that play a more important role in the crystal packing.

Since in an icosahedron the center to vertex distance is about 5% shorter then the vertex to vertex distance, Khanna and Jena[11] suggested substitutional doping of Al_{13} clusters with a smaller atom such as C and Si at the center of an icosahedron in order to obtain a closed packed structure. This would also make this cluster a 40 valence electron system. They obtained significant gain in energy as compared to Al_{13} cluster. However, their calculated center to vertex distance was longer in the doped clusters as compared to the one in Al_{13}. Gong and Kumar[12] subsequently studied several $Al_{12}X$ (X = B, Ga, C, Si, Ge, As, and Ti) clusters and found $Al_{12}C$, $Al_{12}Si$ and $Al_{12}Ge$ to have a substantial gain in energy as shown in Fig. 14. While all these clusters except Ti have about 2 eV HOMO-LUMO gap, $Al_{12}B^-$ is the most strongly bonded in this family. This agrees with the strong abundance of $Al_{12}B^-$ clusters observed by Nakajima *et al*[99]. The main conclusion of this study has been that the chemical bonding plays the dominant role in the stability of these clusters while the atomic relaxation leads to a small gain in the binding energy when a smaller atom such as B, C, Si is sustituted at the center. For Si, a small contraction in the center to vertex distance was obtained[12] as compared to Al_{13} cluster. A similar result was also obtained by Kumar and Sundararajan[46] from CP calculations. Further, Si substitution at the center of an icosahedron was found to be more favorable than at a vertex. This is similar to the result for Na_7Al where Al was found also at the center. A large gain in energy by Si doping may also explain the improved stability of Al-Mn-Si quasicrystals as compared to Al-Mn. On the other hand doping with Ti which also has 4 valence electrons leads to a partially occupied HOMO and a small gain in binding energy as compared to Al_{13}. This is likely to be due to an increase in the Al-Ti bond length. This calculation also suggests that the jellium model may not be applicable in clusters with a transition metal element. An important point which is not resolved by these calculations is whether C at the center is most favorable. It can be noted that though the Al-C bond length is shorter than Al-Al bond, it is still much larger than in the case of Al-C dimer. The large bond length can not be accounted also from an increase in the coordination number of C in an icosahedron. In order to find this, Kumar and Sundararajan[46] have recently done an ab-initio molecular dynamics calculation for $Al_{12}C$. First of all from steepest descent calculations C at the center of an icosahedron is more favorable than C at the vertex by about 1.5 eV. Simulated annealing calculations, however, indicate that carbon tends to have a closed packed environment with 8 atoms while the remaining 4 Al atoms join the Al_8C unit. It is to be noted that $Al_{12}C$ is not a magic cluster in the mass spectrum of Al_NC^- clusters. But Al_7C^-, $Al_{14}C^-$ and $Al_{24}C^-$ are magic which respectively have 26, 47 and 77 valence electrons. None of these correspond to closing of an electronic shell in the SJM. Carbon prefers strongly directional bonding and therefore the SJM may not be appropriate for these clusters. A proper understanding of the carbon

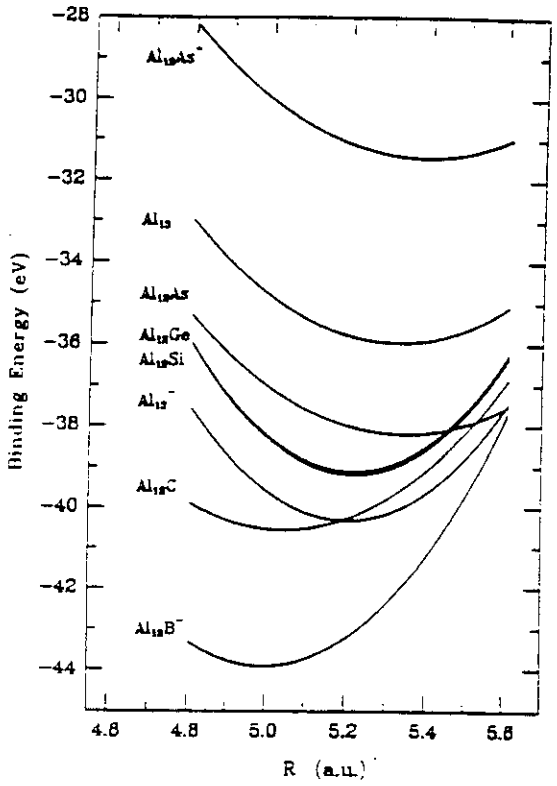

Figure 14 Binding energies of icosahedral $Al_{12}X$ clusters as a function of the center to vertex distance. (After Gong and Kumar[12]).

behaviour would be useful in the study of reactions on clusters. Simulated annealing calculations for these clusters are difficult as very large cut-offs are required to represent the wavefunction but we hope that in the future such calculations can be done in order to understand the structure of these clusters better.

Ga clusters have been studied by Jones[37] and Gong and Tosatti[38]. The overall structural features are similar to those obtained for Al clusters. However, the bonding properties are slightly different due to larger $s-p$ promotion energy in Ga as compared to Al. This leads to weaker sp hybridization and consequently the bond angles in Ga clusters are closer to 90deg arising due to predominantly p bonding. Though Ga is heavier than Al, its valence orbitals are more compact than in Al. This leads to a small contraction in bond length as compared to that in Al clusters. Also though the melting temperature of Ga (29.78deg C) is much smaller than for Al, the binding energies of their clusters are very similar. This reflects the molecular nature of bonding in bulk. For both Ga and Al, there are several 2 and 3 dimensional structures with different spin multiplicities which lie close in energy. This is consistent with their metallic behaviour in bulk.

3.1.5 Sn and Sb clusters

Elements of Group IV and V are very interesting as they exihibit a variety of crystal structures and have differing bonding character in the bulk. Tin has both a metallic (white tin) and a semiconducting (grey tin) phase. Grey tin has the diamond structure, while white tin is body-centered tetragonal with a two atom basis. Kumar[35] has done a calculation for Sn_8 cluster as it has 20 valence electrons and could be expected to be a magic cluster from the point of view of the jellium model. The calculations were done for a few selected geometries and the lowest energy structure is a trigonal bipyramid. The bond length between the base atoms is large and equals 6.50 a.u. whereas the bond length between the apex and base atoms is 4.94 a.u. . This structure is similar to a 5- atom cluster of Ge or Si[24,100] (see below) and therefore its behaviour is more like the clusters of Si. It would be of interest to calculate the structure of Sn_{10} and see if it is the same as for Si_{10} cluster. Also studies on other Sn clusters would be interesting to explore the development of bonding in these clusters.

Clusters of pentavalent elements such as Sb and Bi (all of which are semimetals) have been experimentally studied in detail both using thermal evaporation and subsequent condensation[101] as well as by laser ablation[102]. For Sb clusters produced by thermal evaporation, a very important feature in the mass spectrum is the abundance of Sb_{4n} clusters (Fig. 15a). Also as compared to monomer dissociation in alkali or divalent metal clusters, studies of the fragmentation of such antimony clusters produce evidence of evaporation of tetramers[103]. The abundance spectrum of the thermally evaporated Bi clusters is very different as compared to Sb. There is no particular preference to Bi_{4n} clusters (Fig. 15b). However, clusters of Sb and Bi produced from laser ablation have similar features in the abundance spectrum (Fig. 16). These studies show abundance of clusters with 3, 5 or 7 atoms. Kumar[33]

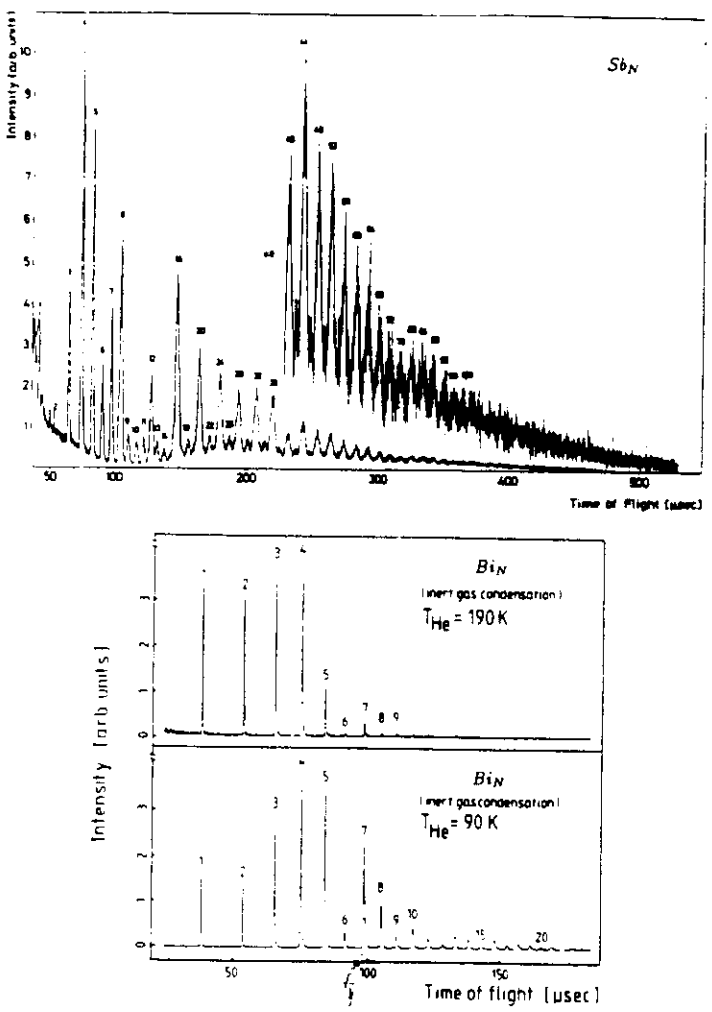

Figure 15. Time of flight mass spectrum of Sb and Bi clusters obtained from thermal evaporation. (After Sattler *et al*[101].)

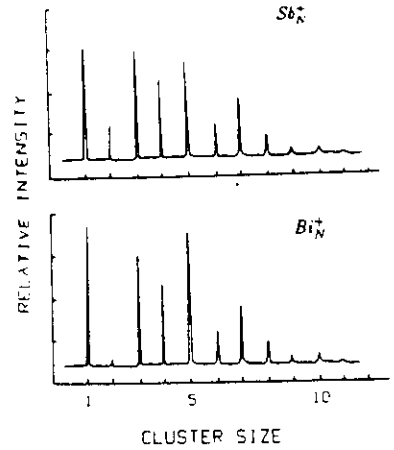

Figure 16: Mass spectrum of (a) Sb and (b) Bi clusters obtained from laser ablation. (After Geusic *et al*[102].

has studied Sb_4 and Sb_8 clusters whereas Sundararajan and Kumar[34] have recently studied some other clusters of Sb. The lowest energy structure of Sb_4 is a regular tetrahedron. A bent rhombus lies about 0.5 eV/atom higher in energy. Sb_4 has 20 valence electrons and can be expected to be a magic cluster as also observed. From this it will appear that the results of the jellium model may be applicable to Sb clusters as Sb_8 has 40 valence electrons which also corresponds to shell closing in SJM and Sb_{12} has 60 valence electrons which can correspond to the magic clusters with 58 electrons. However, recent studies[104] of the photoionization spectra of Sb clusters indicate striking differences in the behaviour of Sb_{4p} , $p > 1$ and other clusters which are not understood. Also the persistence of $4p$ type clusters for larger values of p (upto about 25) indicates a different bonding character in these clusters. Detailed calculations by Kumar[33] on Sb_8 clusters show that a cube, two fused bent rhombuses, and a capped octahedron are not even stable against two isolated tetrahedra (Fig. 17a-c). Simulated annealing calculations for this cluster result in a structure having two tetrahedra weakly interacting with each other (Fig. 17e) in confirmity with the well known result that thermal heating of Sb leads to evaporation of Sb_4 units. Another SA calculation with a different starting configuration and heat treatment leads to a different structure (Fig. 17d) which can be described as a bent rhombus interacting with a distorted tetrahedron. This structure lies only 0.117 eV higher in energy than the structure with two weakly (van der Waals type) interacting tetrahedra. It is well known that LDA is not good for describing van der Waals interactions and therefore binding energy of the two tetrahedra is

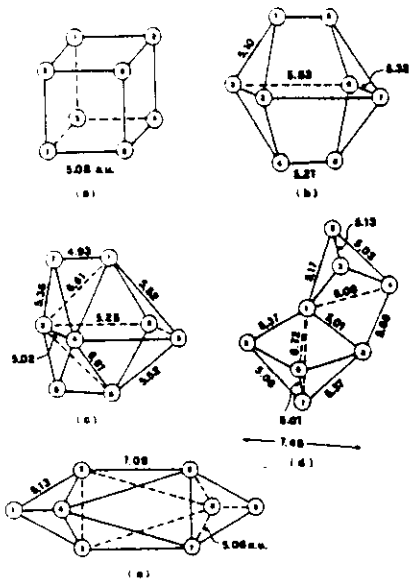

Figure 17: Different isomers of Sb_8. (a)-(c) are not stable against two isolated tetrahedra. (e) has the lowest energy and is nearly degenerate with (d). (After Kumar[33]).

likely to be overestimated. Therefore these two isomers can be treated to be nearly degenerate. These calculations indicated the importance of bent rhombus structure for larger clusters and suggested that the molecular architecture could depend upon nucleation conditions.

Results on 2- 5 atom Sb clusters are shown in Fig. 18. For Sb_5 a square pyramid has the lowest energy while for Sb_6 a prism has the lowest energy. The Kohn-Sham eigenvalues are shown in Fig. 19. It can be noted that for 3, 5 and 7 atom clusters there is a large gap between the highest and the next occupied levels. This explains the abundance of Sb_3^+, Sb_5^+ and Sb_7^+ clusters in the laser ablation experiments in which the growth is expected to be atom by atom. Simulations on 7-atom cluster show that as the cluster is cooled, it undergoes fast isostructural transformations by making and breaking bonds (Fig. 20). Such dynamical aspects may play an important role in understanding reactions on clusters. Also the finite temperature studies help to get information about other low lying structures which

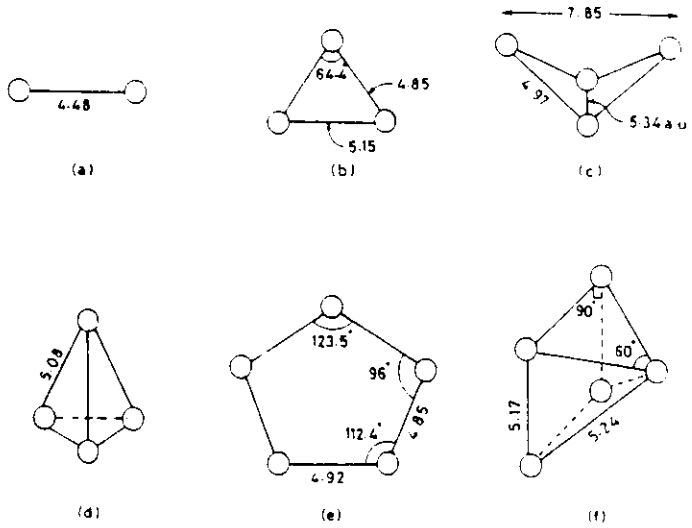

Figure 18: Low energy structures of Sb_2 - Sb_5 clusters. Tetrahedron and square pyramid are the lowest energy structures for Sb_4 and Sb_5. (After Sundararajan and Kumar[34]).

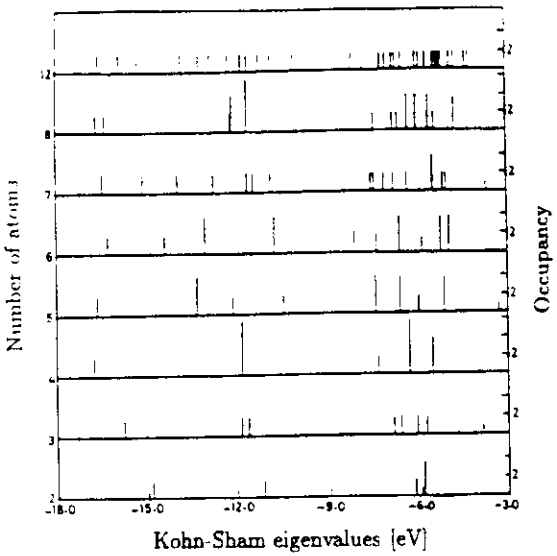

Figure 19: Kohn-Sham eigenvalues of Sb clusters. Note the large gap between the highest and the next occupied level for Sb_3, Sb_5 and Sb_7. (After Sundararajan and Kumar[34]).

the cluster may visit during the simulation. Unlike in bulk, it is not just thermal vibrations, but also much below the bulk melting temperature there could be important (dynamical) structural transformations in clusters which could be decisive in determining their properties. From Fig. 20 one can see that while above 600 K a structure with two fused bent rhombuses has a large basin of attraction, the low temperature structure is a bent rhombus interacting with a triangle.

From the above discussion it is clear that the jellium model is not applicable to Sb clusters and the bonding is strongly directional. Also unlike in other metal clusters where fragmentation is predominantly of monomers, the fragmentation channels for different clusters are different for Sb clusters[34].

3.2 Clusters of semiconductors and other materials

3.2.1 Si, Ge, GaAs, GaP and AlAs

Andreoni and coworkers[24,43,100] have studied these clusters from the CP method. As expected Si and Ge clusters have similar structures. An important aspect of the structure of these clusters is that these are closer packed as compared to more open

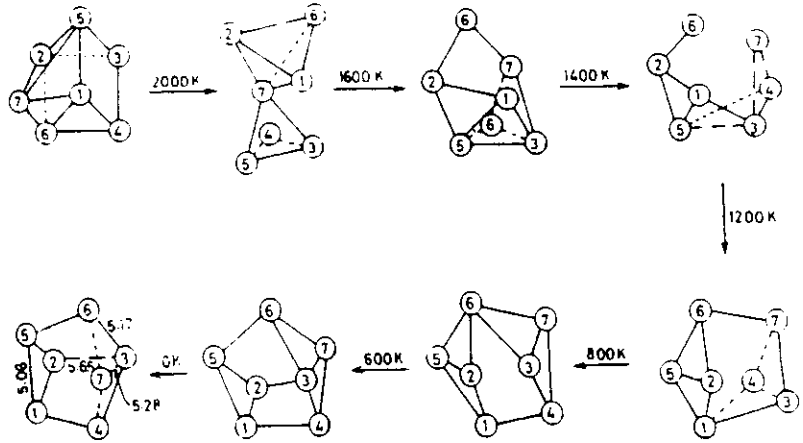

Figure 20: Snap-shots of some structures at different temperatures for Sb_7. Note the isostructural transformations during simulated annealing. (After Sundararajan and Kumar[34]).

diamond structure in the bulk. It is of considerable interest to know when directional bonding starts playing an important role in these clusters. Several efforts have been devoted to answer this question. Extensive calculations[105] for Si clusters with upto 45 atoms show no sign of bulklike features in the structure. Si was the first example where the advantage of simulated annealing became evident when an entirely new structure (tetracapped trigonal prism, same as for Mg_{10}) was found to be of lowest energy. The growth pattern of Si clusters is rather complex and no common seed can be identified. Si_8 and Ge_8 have the same structure as the one for Sn_8 which suggest directional bonding but the larger clusters seems to behave more like metal clusters. Si_7 is a pentagonal bipyramid as Mg_7. Si_8 is a bicapped octahedron (two opposite faces capped) and Si_9 is a strongly reconstructed structure and is shown in Fig. 21. Si_{10} and Ge_{10} are tetracapped trigonal prisms similar to Mg_{10} whereas Si_{13} is neither a cubooctahedron nor an icosahedron. Its lowest energy structure is also shown in Fig. 21. An important message of these calculations is that the semiempirical potentials available for Si may not be suitable for the representation of the potential energy surface of microclusters[106].

A few calculations have also been done for Ga_NAs_N, Ga_NP_N and Al_NAs_N clusters[43] containing upto 10 atoms. Some of their isomers have similarity with those of Si and Ge clusters but there are significant differences due to two species and anion-anion bonds. All the atoms in these clusters are undercoordinated as

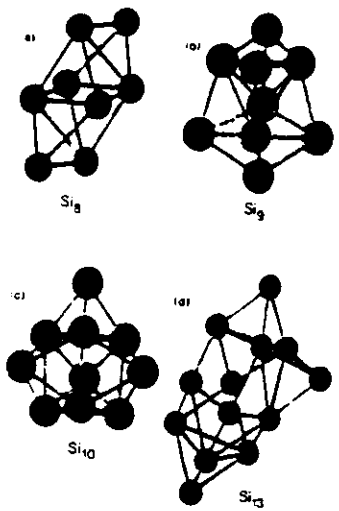

Figure 21: Lowest energy structures of 8-, 9-, 10-, and 13- atom Si clusters. (After Andreoni[24]).

compared to bulk and therefore the chemical bonding and order differs from bulk in these small aggregates. Bonds between unlike atoms are more prevalent in AlAs as the Al-As bond is more ionic than the Ga-As bond whereas in Ga-P clusters there is a preference for Ga atoms to segregate at the surface. For Ga_6As_6 cluster, though the lowest energy structure is a distorted bicapped dodecahedron, a tetracapped trigonal prism is nearly degenerate. This is an interesting result because this as well as Si_{10} and Ge_{10} clusters have 40 valence electrons each. This is a magic number in the shell model. The occurrence of the same structure for Mg_{10} cluster makes us believe that *there may be some unique structures which are either lowest or lie very close in energy with the lowest energy structures for magic clusters for which directional bonding plays a less important role.* Thus studies of low lying isomers may provide useful information about the chemical bonding in small clusters.

3.2.2 B, S, Se, P, C

Boron, a trivalent element, has a tendency for very strong directional bonding. The abundance specturm of boron clusters produced from a laser ablation source[107] shows prominent stability of positively charged 5, 10 and 13 atom clusters. This behaviour is different from clusters of aluminium and is in conformity with the observation of several crystalline phases of boron and a large variety of

alloys in which atomic distribution is rather complicated[108]. One of the most prominent units in these structures is the B_{12} empty center icosahedron which has five fold rotational symmetry. However, small distortions can lead to lower symmetries compatible with crystalline order. Strong directional bonding in boron forces it to develop a complicated three dimensional crystalline order, often with large unit cells. One can then ask the question whether such icosahedral units would also be favorable for clusters. Laser ablation experiments[107] showed 12 atom cluster not to be magic. Other experiments[109] suggest that B_{13}^+ does not react with H_2 or H_2O whereas other clusters are reactive. High stability of B_{13}^+ was considered to be due to an icosahedral cage with an atom at the center. However, here it may be noted that for aluminium, negatively charged 13 atom cluster was most abundant. Kawai and Weare[42], have done ab-initio molecular dynamics study of B_{12} and B_{13} clusters. Their studies showed that an icosahedron is not even a local minimum for B_{13}. The atom at the center comes out of the cage and the lowest energy structure consists of a pentagon and a hexagon layer. The singly occupied HOMO and the next occupied level are well separated and this leads to the stability of B_{13}^+. For B_{12}, though an icosahedron is a local minimum, it has dangling bonds and one of the atoms is very loosely bonded. Simulated annealing calculations lead to an open structure which is significantly lower in energy due to removal of the dangling bonds. The existance of icosahedral clusters in bulk phases has therefore been suggested to be due to the formation of strong intericosahedral links. These calculations also indicated the inappropriateness of a SJM for these clusters. The same conclusion can be drawn from the work of kumar and Sundararajan[45] who studied carbon substitution at the center of the icosahedral B_{13} cluster. Similar to B_{13}, carbon comes out of the center and the icosahedral structure is not energetically favorable.

Jones and coworkers have made extensive calculations for S^{27}, Se^{28} and P^{30} clusters. In some of these cases it is possible to compare the results with the spectroscopic data available for the structure. These results give confidence in the simulated annealing procedure as the calculated bond lengths and angles agree remarkably with the experimental values. The atomization energies are ,however, overestimated which is due to the use of the LDA. As there is a large amount of information regarding the structure of these molecules, the reader is advised to consult the original papers for details. It would be worth to mention that similar to Sb_4, P_4 is also a regular tetrahedron. However, contrary to widespread belief, the most stable structure of P_8 is not cubic. It is a structure with C_{2v} symmetry and its energy lies 0.47 eV below that of two isolated P_4 tetrahedra. A roof-shaped tetramer (bent rhombus) is a prominent structural unit in the low-lying states of P_5, P_6, P_7 and P_8 clusters as it was also found for Sb clusters. However, the growth pattern in the two cases is different.

Some calculations have also been done[29] for C_4 and C_{10} clusters for which the structures are respectively a linear chain and a ring. Due to more localized orbitals these calculations require use of very large energy cutoff in the plane wave expansion and therefore are very expensive to do. However, due to recent excitement in fullerenes, several efforts are going on to study large clusters of carbon with 60 or

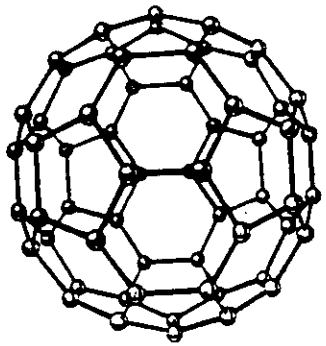

Figure 22: Truncated icosahedral structure of C_{60} cluster.

more atoms. C_{60} cluster (Fig. 22) has a football structure with 12 pentagons and 20 hexagons. There are two bond lengths (1.40 and 1.45 $\AA$) as obtained from NMR data[110]. The bonds sharing two hexagons form double bonds and are short whereas the bonds sharing a pentagon and a hexagon are single bonds and are longer. All atoms have identical environment. Calculations by Feuston *et al*[40] produce these bond lengths to be 1.39 and 1.45 $\AA$ in very good agreement with the NMR experiments. As it is possible to do calculations at finite temperatures, they studied the structural changes and vibrational and average electronic density of states at 450 K. The fullerene structure of C_{60} was found to be very stable and the average structural parameters change by at most 0.01 $\AA$. The calculated vibrational frequencies 530, 555, 1105 and 1345 cm^{-1} are in close agreement with 527.1, 570.3, 1169.1, 1406.9 cm^{-1} obtained from infra-red spectroscopy experiments[111]. Due to the observation of superconductivity in doped solid C_{60}, studies of the doped fullerenes are of interest. Kohanoff *et al*[41] and Laasonen *et al*[41] have studied hydrogen and La doping of fullerenes and their effects on the atomic and electronic structure of the fullerenes. Due to the difficulty in doing CP calculations with plane wave basis, efforts have been made[112,113] to use schemes based on a tight binding Hamiltonian. This has allowed the study of the relative stability of different isomers of carbon clusters upto about 100 atoms. Fig. 23 shows the heat of formation of carbon clusters for 20-94 atoms obtained by Wang *et al*[43] from tight-binding molecular dynamics calculations. It can be seen that the heat of formation slowly approaches to the value of graphite almost monotonically. However, C_{60} shows marked increase due to its high symmetry and the distribution of strain due to curvature uniformly.

Efforts are also being made to understand the properties of solids made from such large clusters. Zhang *etal*[114] have studied the structural properties of solid C_{60}

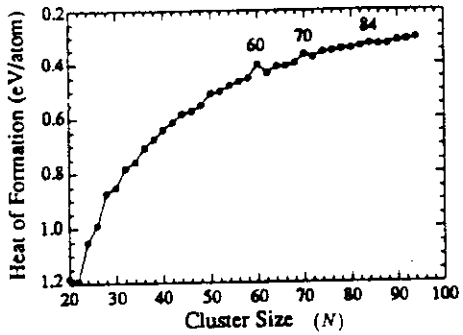

Figure 23: The heat of formation of carbon fullerenes relative to that of graphite as a function of the cluster size. (After Wang *et al*[113].)

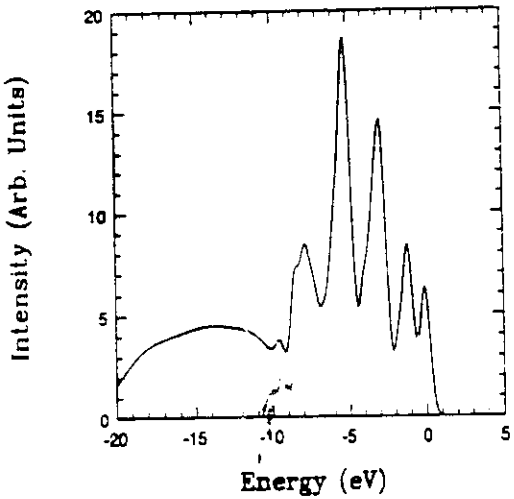

Figure 24: Gaussian broadened electron energy spectrum of solid C_{60}. (After Kumar[118].)

with a fcc structure and found the bond lengths to be 1.40 and 1.45 $\AA$ i.e. very little change from the values in the cluster. Kumar[118] has also done a similar calculation with 29 Ry. cutoff and find some anisotropy in the bond lengths due to different environments of the sites in the solid phase as compared to one in the isolated cluster. In particular there are three different environments of carbon atoms in the fcc structure. The double bonds have one bond length which is equal to 1.404 $\AA$, whereas the single bonds have three slightly different values. These are 1.449, 1.454 and 1.462 $\AA$. 24 atoms have their nearest neighbour bond lengths to be 1.404, 1.449 and 1.454 $\AA$. The other 24 have 1.404, 1.449 and 1.462 $\AA$ and the remaining 12 have 1.404, 1.454 and 1.454 $\AA$. The calculated electronic energy spectrum is shown in Fig. 24 which is good agreement with the photoemission data[118]. Experimentally[116,117] an orientational ordering of the C_{60} balls has been found below 249 K. This leads to a $Pa\bar{3}$ structure. Since the number of atoms in this structure become four times than in the fcc structure per unit cell, CP calculations becomes very difficult. However, further work on these and doped fullerenes is in progress in some laboratories.

4. Outlook

Fairly good amount of work has been carried out in recent years using the Car-Parrinello method for clusters of metals, semiconductors and other elements like B, C, S, Se, P etc. The simulated annealing technique has given a new thrust in the search for the ground state structures of clusters. The structures and the vibrational frequencies calculated with this technique are in general good agreement with experiments wherever results are available. Interesting information has been obtained on the dynamical changes in the structure at finite temperatures and the bonding properties for some systems but more work on larger clusters and other systems would be useful with the availability of better computational facilities and algorithms which scale linearly with system size.[119]. Also it would be most interesting to apply this technique to problems related to reactions on clusters and to other mixed clusters. From the point of view of applications, clusters of transition metals are very important and recent developments in pseudopotentials[120] and their implementation in the Car-Parrinello method[121] is a step forward in this direction and we hope to see applications of this to some transition metal clusters in the near future. Studies of the magnetic properties are few but hopefully these developments would lead to better understanding of magnetic properties of transition metal clusters. It would be desirable to develop more efficient algorithms for systems having d electrons or more localized orbitals such as in C or O. In the next few years we hope to see important developments in these directions.

5. Acknowledgements

I would like to express my sincere thanks to my collaborators R. Car, V. Sundararajan, X. G. Gong, I. Garzon, G. Pastore and W. Andreoni whose cooperation has led to much of the work presented here and to G. Chiarotti , G. Galli and K. Laasonen with whom I have enjoyed several fruitful discussions.

6. References

1. *Microclusters*, Eds. S.Sugano, Y. Nishina and S. Ohnisi, Springer, Berlin (1987).
2. *Physics and Chemistry of Finite Systems: From Clusters to Crystals*, Vol. 1 and 2, Eds. P. Jena, S. N. Khanna and B.K. Rao, Kluwer Academic Publishers, Netherlands (1992).
3. *Clusters and Fullerenes*, Eds. Vijay Kumar, T.P. Martin and E. Tosatti, World Scientific (1993).
4. Articles in *Proceedings of the Fourth International Meeting on Small Particles and Inorganic Clusters*, Marseille, France (1988), published in Z. Phys. D12, (1989).
5. Articles in *Proceedings of the Fifth International Meeting on Small Particles and Inorganic Clusters*, Konstanz, Germany (1988), published in Z. Phys. D19 and 20 , (1991).
6. W. Krätschmer, D.L. Lowell, K. Fostiropoulos, and D.R. Huffman, Nature 347, 354 (1990); for C_{60} cluster see H. W. Kroto, J. R. Heath, S. C. O'Brien, R. F. Curl and R. E. Smalley, Nature, 318, 162 (1985).
7. A.F. Hebard *et al*, Nature 350, 600 (1991).
8. M.J. Rosseinsky *et al*, Phys. Rev. Lett. 66, 2830 (1991); K. Holczer *et al*, Science 252,1154 (1991).
9. K. Tanigaki *et al*, Science 352, 222 (1991).
10. B. C. Guo, K. P. Kerns and A. W. Castleman, Jr., Science 255, 1411 (1992); B. C. Guo, S. Wei, J. Purnell, S. Buzza and A. W. Castleman, Jr., Science 256,515 (1992).
11. S. N. Khanna and P. Jena, Phys. Rev. Lett. 69, 1664 (1993).
12. X. G. Gong and Vijay Kumar, Phys. Rev. Lett. 70, 2078 (1993).
13. F. D. Weiss, J. L. Elkind, S. C. O'Brien, R. F. Curl and R. E. Smalley, J. Am. Chem. Soc., 110, 4464 (1988); Y. Chai, T. Guo, C. Jin, R. E. Haufler, L. P. F. Chibante, J. Fure, L. Wang, J. M. Alford and R. E. Smalley, J. Phys. Chem. 95, 7564 (1991).
14. S. Iijima, Nature (London) 354, 56 (1991).
15. D. Ugarte in Ref. 3 pp. 231.
16. P. Ballone, W. Andreoni, R. Car and M. Parrinello, Phys. Rev. Lett. 60, 271(1988).

17. K. Rademann, B. Kaiser, U. Even and F. Hensel, Phys. Rev. Lett. **59**, 2319 (1987); K. Rademann, Ber. Bunsenges. Phys. Chem. **93**, 653 (1989); C. Brechignac, M. Broyer, P. Cahuzac, G. Delacretaz, P. Labastie, J.P. Wolf and L. Woste, Phys. Rev. Lett. **60**,275 (1988).

18. See J. H. Sinfelt, Rev. Mod. Phys. **51**, 569 (1979).

19. R.L. Whetten *et al*, Phys. Rev. Lett. **54**, 1494 (1985).

20. R.E. Leuchtner, A.C. Harms and A.W. Castleman, Jr., J. Chem. Phys. **91**, 2753 (1989).

21. T. P. Martin, T. Bergmann, H. Göhlich and T. Lange, Chem. Phys. Lett. **176**, 343 (1991); T. P. Martin, U. Näher and H. Schaber, Chem. Phys. Lett. **199**, 470 (1992).

22. W. A. de Heer, W. D. Knight, M. Y. Chou and M. L. Cohen, Solid State Phys. Vol.**40**, Eds. H. Ehrenreich and D. Turnbull, Academic Press (1987).

23. R. Car and M. Parrinello, Phys. Rev. Lett. **55**, 2471 (1985).

24. See for a brief review W. Andreoni, in Ref. 5, **D19**, pp. 31; also a finite temperature study of a few selected clusters of Na, Mg and Si can be found in U. Röthlisberger and W. Andreoni, Z. Phys. **D20**, 243 (1991).

25. Vijay Kumar in *Atomic and Molecular Physics*, Ed. A. P. Pathak, Narosa (1992), pp. 90.

26. D. Hohl, R. O. Jones, R. Car and M. Parrinello, Chem. Phys. Lett. **139**, 540 (1987).

27. D. Hohl, R. O. Jones, R. Car and M. Parrinello, J. Chem. Phys. **89**, 6823 (1988).

28. P. Ballone, W. Andreoni, R. Car and M. Parrinello, Europhys. Lett. **8**, 73 (1989).

29. U. Röthlisberger and W. Andreoni, J. Chem. Phys. **94**, 8129 (1991).

30. R.O. Jones and D. Hohl, J. Chem. Phys. **92**, 6710 (1990).

31. R. Kawai and J. H. Weare, Phys. Rev Lett. **65**, 80 (1990).

32. Vijay Kumar and R. Car, in Ref.5, **D19**, pp. 177; Phys. Rev. **B44**, 8243 (1991).

33. Vijay Kumar, Phys. Rev. **B48**, 8470 (1993).

34. V. Sundararajan and Vijay Kumar, unpublished.

35. Vijay Kumar in Ref. 3 pp. 97.

36. R. O. Jones, Phys. Rev. Lett. **67**, 224 (1991); J.-Y. Yi, D. J. Oh, J. Bernholc and R. Car, Chem. Phys. Lett. **174**, 461 (1990); J.-Y. Yi, D. J. Oh and J. Bernholc, Phys. Rev. Lett. **67**, 1594 (1991).

37. R. O. Jones, J. Chem. Phys. **99**, 1194 (1993).

38. X. G. Gong and E. Tosatti, Phys. Lett. **A 43**, 369 (1992).

39. W. Andreoni, D. Scharf and P Giannozzi, Chem. Phys. Lett. **173**, 449 (1990).

40. B. Fueston, W. Andreoni, E. Clementi and M. Parrinello, Phys. Rev. **B44**, 4056 (1991); Q.-M. Zhang et al in Ref. 3, pp. 83; Vijay Kumar (unpublished).

41. J. Kohanoff, W. Andreoni and M. Parrinello, Chem. Phys. Lett. **198**, 472 (1992); K. Laasonen, W. Andreoni and M. Parrinello, Science (in press).

42. R. Kawai and J. H. Weare, J. Chem. Phys. **95**, 1151 (1991).

43. W. Andreoni, Phys. Rev. **B 45**, 4203 (1992).

44. U. Röthlisberger and W. Andreoni, Chem. Phys. Lett. **198**, 478 (1992) and in Ref. 3 pp. 91.

45. Vijay Kumar and V. Sundararajan, unpublished.

46. R. Car and M. Parrinello, in *Simple Molecular Systems at Very High Density*, Eds. A. Polian, P. Loubeyre and N. Boccara, (NATO ASI Series, Plenum, New York (1989)).

47. D.K. Remler and P.A. Madden, Mol. Phys. **70**, 921 (1990).

48. G. Galli and A. Pasquarello, preprint.

49. M. C. Payne, M. P. Teter, D. C. Allan, T. A. Arias and J. D. Joannopoulos, Rev. Mod. Phys. **64**, 1045 (1992).

50. P. Hohenberg and W. Kohn, Phys. Rev. **136**, 864B (1964).

51. W. Kohn and L.J. Sham, Phys. Rev. **140**, 1133A (1965).

52. R.O. Jones and O. Gunnarsson, Rev. Mod. Phys. **61**, 689 (1989).

53. V. L. Moruzzi, J. F. Janak and A. R. williams, *Calculated Electronic Properties of Metals*, Pergamon, New York (1978).

54. H. Hellmann, *Einfuhrung in die Quantenchemie*, Deuticke, Leipzip (1937); R. P. Feynman, Phys. Rev. **56**, 340 (1939).

55. G. W. Fernando, G. X. Qian, M. Weinert and J. W. Davenport, Phys. Rev. **B40**, 7985 (1989); M. R. Pederson and K. A. Jackson, Phys. Rev. **43**, 7312 (1991).

56. S. Nose, J. Chem. Phys. **81**,511 (1984).

57. P. E. Blöchl and M. Parrinello. Phys. Rev. **B45**, 9413 (1992).

58. A. Williams and J. Soler, Bull. Am. Phys. Soc. **32**, 562 (1987); J. M. Soler and A. R. Williams, Phys. Rev. **B40**, 1560 (1989); ibid. B42, 9728 (1990).

59. See for a recent review, W. E. Pickett, Comput. Phys. Rep. **9**, 115 (1989).

60. D. J. Chadi and M. L. Cohen, Phys. Rev. **B8**, 5747 (1973); H. J. Monkhorst and J. D. Pack, Phys. Rev. **B13**, 5188 (1976).

61. G. B. Bachelet, D. R. Hamann and M. Schluter, Phys. Rev. **B26**,4199 (1982).

62. N. Troullier and J. L. Martins, Phys. Rev. **B43**, 1993 (1991); G. Kerker, J. Phys. **C13**, L189 (1980); D. R. Hamann, Phys. Rev. B40, 2980 (1989); E. L. Shirley, D. C. Allan, R. M. Martin and J. D. Joannopoulos, Phys. Rev. **B40**, 3652 (1989).

63. L. Kleinman and D. M. Bylander, Phys. Rev. Lett. **48**, 1425 (1982); see also P. E. Blöchl, Phys. Rev. **B41**, 5414 (1990); M. Y. Chou, Phys. Rev. **B45**, 11465 (1992).

64. X. Gonze, P. Käckell and M. Scheffler, Phys. Rev. B41, 12264 (1990); X. Gonze, R. Stumpf and M. Scheffler, Phys. Rev. B44, 8503 (1991).

65. J. Ihm, A. Zunger and M. L. Cohen, J. Phys. **C12**, 4409 (1979); P. Bagno, L. F. Dona Dalle Rose and F. Toigo, Adv. Phys. **40**, 685 (1991).

66. In fact in the formulation of Bachelet et al (Ref. 61), the ionic pseudopotential is explicitly written as a core term coming from a Gaussian distribution and the remaining part as we have expressed in Eq. (13).

67. S. Kirkpatrick, C. D. Gelatt, and M. P. Vecchi, Science **220**, 671 (1983).

68. W. D. Knight, K. Clemenger, W. A. de Heer, W. A. Saunders, M. Y. Chou and M. L. Cohen, Phys. Rev. Lett **52**, 2141 (1984).

69. W. A. Saunders, K. Clemenger, W. A. de Heer and W. D. Knight, Phys. Rev. **B32**, 1366 (1985); M. M. Kappes, M. Schär, P. Radi and E. Schumacher, J. Chem. Phys. **84**, 1863 (1986).

70. M. M. Kappes, P. Radi, M. Schär and E. Schumacher, Chem. Phys. Lett. **115**, 11(1985); M. M. Kappes, M. Schar and E. Schumacher, J. Phys. Chem. **91**, 658 (1987).

71. I. Katakuse, I. Ichihara, Y.Fujita, T. Matsuo, T. Sakurai and H. Matsuda, Int. J. Mass Spectrom. Ion Proc. **67**, 229 (1985).

72. I. Katakuse, T. Ichihara, Y. Fujita, T. Matsuo and H. Matsuda, Int. J. Mass Spectrom. Ion Proc. **69**, 109 (1986).

73. See Refs. 22 and 69;

74. C. Brechignac, Ph. Cahuzac, F. Carlier, M. de Frutos and J. Leygnier, J. Chem. Soc. Faraday Trans. **86**, 2525 (1990).

75. W. D. Knight, K. Clemenger, W. A. de Heer and W. A. Saunders, Phys. Rev. **B31**, 2539 (1985).

76. P. Ballone and G. Galli, Phys. Rev. **B42**, 1112 (1990); ibid. **B40**, 3563(1989).

77. W. Eckert, Phys. Rev. **B29**,1558 (1984).

78. See, for example, R. M. Eisberg, *Fundamentals of Modern Physics*, p. 407, Wiley, New York, 1967.

79. See, for example H. Frauenfelder and E. M. Henley, *Subatomic Physics*, Chapter 15, Prentice-Hall, englewood Cliffs, New Jersey, 1974.

80. M.Y. Chou, A. Cleland and M. L. Cohen, Solid State Commun. 52, 645 (1984); M. Y. Chou and M. L. Cohen, Phys. Lett. **A113**, 420 (1986).

81. K. Clemenger, Phys. Rev. **B32**, 1359 (1985).

82. M. M. Dacorogna and M. L. Cohen, Phys. Rev. **B 34**, 4996 (1986).

83. V. Bonacic-Koutecky, P. Fantucci and J. Koutecky, Phys. Rev. **B37**, 4369(1988).

84. I. Garzon, Vijay Kumar, G. Pastore and W. Andreoni, unpublished.

85. E. S. Fois, J. I. Penman and P. A. Madden, J. Chem. Phys. (1993)

86. Vijay Kumar, Phys. Rev. **B23**, 3756 (1981); Surf. Sci. **84**, L231 (1979).

87. V. de Coulon, P. Delaly, P. Ballone, J. Buttet and F. Reuse, in Ref. 5, **D19**, pp. 173.

88. K.P.Huber and G. Herzberg, *Molecular Spectra and Molecular Structure. IV Constants of Diatomic Molecules* (Van Norstrand Reinhold, New York, 1974).

89. Ballone et al, Ref. 5.

90. F. Reuse, S.N. Khanna, U. de Coulon and J. Buttet, Phys. Rev. **B41**, 11743 (1990).

91. G. Pacchioni, W. Pewestorf and J. koutecky, Chem. Phys. **83**, 261 (1984).

92. B. Delley, D. E. Ellis, A. J. Freeman, E. J. Barends and D. Post, Phys. Rev. **B27**, 2132 (1983).

93. V. Kumar, unpublished.

94. S. G. Louie, S. Froyen and M. L. Cohen, Phys. Rev. **B26**, 1738 (1982).

95. W. B. Pearson, *The Crystal Chemistry and Physics of Metals and Alloys*, Wiley, New York 1973.

96. A. Nakajima, T. Kishi, T. Sugioka, Y. Sone and K. Kaya, Chem. Phys. Lett. **177**, 297 (1991).

97. V. Kumar, in Proc. Adriatico Annversary Conference on 'Quasicrystals', Eds. M. Jaric and S. Lundquist, World Scientific(1990).

98. F. C. Frank and J. S. Kaspar, Acta Crystallogr. **11**, 184 (1958); ibid. **12**, 483 (1959).

99. A. Nakajima, T. Kishi, T. Sugioka and K. Kaya, Chem. Phys. Lett. **187**, 239 (1991).

100. P. Ballone, W. Andreoni, R. Car and M. Parrinello, Phys. Rev. Lett. **60**, 271 (1988).

101. K. Sattler, J. Muhlbach and E. Recknagel, Phys. Rev. Lett. **45**, 821 (1980). K. Sattler in *Current Topics in Materials Science*, Vol. **20**, Ed. E. Kaldis, North Holland (1985).

102. M. E. Geusic, R. R. Freeman and M. A. Duncan, J. Chem. Phys. **89**, 223 (1988).

103. D. Rayane, P. Melinon, B. Tribollet, B. Cabaud, A. Hoareau, and M. Broyer, J. Chem. Phys. **91**, 3100 (1989).

104. C. Brechignac, M. Broyer, Ph. cahuzac, M. de Frutos, P. Labastie, and J. -Ph. Roux, Phys. Rev. Lett. **67**, 1222 (1991).

105. W. Andreoni, private communication.

106. W. Andreoni and G. Pastore, Phys. Rev. **B41**, 10243 (1990).

107. L. Hanley, J. L. Whitten and S. L. Anderson, J. Phys. Chem. **90**, 5803 (1988).

108. D. Emin, T. Aselage, C. L. Beckel, I. A. Howard and C. Wood, Eds. AIP Conf. Proc. **140**, *Boron-Rich Solids* (AIP, New York, 1986).

109. S. A. Ruatta, L. Hanley and S. L. Anderson, J. Chem. Phys. **91**, 226 (1989); P. A. Hintz, S. A. Ruatta and S. L. Anderson, J. Chem. Phys. **92**, 292 (1990).

110. C. S. Yannoni, P. P. Bernier, D. S. Bethune, G. Meijer, and J. R. Salem, J. Am. Chem. Soc. **113**, 3190 (1991).

111. C. I. Frum, R. Engleman, H. G. Hedderich, P. F. Bernath, L. D. Lamb and D. R. Huffman, Chem. Phys. Lett. **176**, 504 (1991).

112. K. Laasonen and R. M. Nieminen, J. Phys. **CM2**, 1509 (1990).

113. B. L. Zhang, C. Z. Wang, K. M. Ho, J. Chem. Phys. **96**,7183 (1992); Wang et al. in Ref. 3 pp. 249.

114. Q.-M. Zhang, J. -Y. Yi and J. Bernholc, Phys. Rev. Lett. **66**, 2633 (1991).

115. V. Kumar, unpublished.

116. P. A. Heiney, J. E. Fischer, A. R. McGhie, W. J. Romanow, A. M. Denenstein, J. P. McCauley, Jr., A. B. Smith,III and D. E. Cox, Phys. Rev. Lett. **66**, 2911 (1991).

117. W. I. F. David *et al*, Nature **353**, 147 (1991).

118. P. J. Benning, J. L. Martins, J. H. Weaver, L. P. F. Chibante and R. E. Smalley, Science **252**, 1418 (1991).

119. G. Galli and M. Parrinello, Phys. Rev. Lett. **69**, 3547 (1992).

120. D. Vanderbilt, Phys. Rev. **B41**, 7892 (1990).

121. A. Pasquarello, K. Laasonen, R. Car, C. Lee and D. Vanderbilt, Phys. Rev. Lett. **69**, 1982 (1992).